Impact of HO_2 aerosol uptake on radical levels and O_3 production during summertime in Beijing

Joanna E. Dyson[1], Lisa K. Whalley[1,2]*, Eloise J. Slater[1,a], Robert Woodward-Massey[1], Chunxiang Ye[3], James D. Lee[4,5], Freya Squires[4,b], James R. Hopkins[4,5], Rachel E. Dunmore[4], Marvin Shaw[4,5], Jacqueline F. Hamilton[4], Alastair C. Lewis[4,5], Stephen D. Worrall[6], Asan Bacak[7], Archit Mehra[8,c], Thomas J. Bannan[8], Hugh Coe[8,9], Carl J. Percival[10], Bin Ouyang[11], C. Nicholas Hewitt[11], Roderic L. Jones[12], Leigh R. Crilley[13], Louisa J. Kramer[14], W. Joe. F. Acton[14], William J. Bloss[14], Supattarachai Saksakulkrai[14], Jingsha Xu[14,d], Zongbo Shi[14], Roy M. Harrison[14,e], Simone Kotthaus[15,16], Sue Grimmond[15], Yele Sun[17], Weiqi Xu[17], Siyao Yue[17,18,19], Lianfang Wei[17,19], Pingqing Fu[17,18], Xinming Wang[20], Stephen R. Arnold[21], Dwayne E. Heard[1]*

[1] School of Chemistry, University of Leeds, LS2 9JT, UK.

[2] National Centre of Atmospheric Science, University of Leeds, LS2 9JT, UK.

[3] College of Environmental Sciences and Engineering, Peking University, Beijing, 100871, China.

[4] Wolfson Atmospheric Chemistry Laboratories, Department of Chemistry, University of York, Heslington, York, YO10 5DD, UK.

[5] National Centre of Atmospheric Science, University of York, Heslington, York, YO19 5DD, UK.

[6] Aston Institute of Materials Research, School of Engineering and Applied Science, Aston University, Birmingham, B4 7ET, UK.

[7] Turkish Accelerator and Radiation Laboratory, Ankara University Institute of Accelerator Technologies, Atmospheric and Environmental Chemistry Laboratory, Gölbaşi Campus, Ankara, Turkey.

[8] Centre of Atmospheric Sciences, School of Earth and Environmental Sciences, University of Manchester, Manchester, M13 9PL, UK.

[9] National Centre for Atmospheric Sciences, University of Manchester, Manchester, M13 9PL, UK.

[10] Jet Propulsion Laboratory, California Institute of Technology, Pasadena, CA, USA.

[11] Lancaster Environment Centre, Lancaster University, Lancaster, LA1 4YW, UK.

[12] Department of Chemistry, University of Cambridge, Cambridge, UK.

[13] Department of Chemistry, York University, Toronto, ON, M3J 1P3, Canada.

[14] School of Geography, Earth and Environmental Sciences, University of Birmingham, Birmingham, B15 2TT, UK.

[15] Department of Meteorology, University of Reading, Reading, UK.

[16] Institut Pierre Simon Laplace, École Polytechnique, Palaiseau, France.

[17] State Key Laboratory of Atmospheric Boundary Layer Physics and Atmospheric Chemistry, Institute for Atmospheric Physics, Chinese Academy of Sciences, Beijing 100029, China.

[18] Institute of Surface-Earth System Science, School of Earth System Science, Tianjin University, Tianjin 300072, China.

[19] Minerva Research Group, Max Planck Institute for Chemistry, 55128 Mainz, Germany.

[20] State Key Laboratory of Organic Geochemistry, Guangzhou Institute of Geochemistry, Chinese Academy of Sciences, Guangzhou, 510640, China.

[21] School of Earth and Environment, University of Leeds, LS2 9JT, UK.

[a]now at: The Hut Group, Unit 1 Icon Manchester, Manchester Airport, WA15 0AF, UK.

[b]now at: British Antarctic Survey, Cambridge, CB3 0ET, UK.

[c]now at: Chaucer, Part of Bip Group, 10 Lower Thames Street, London, EC3R 6EN[d]now at: Beijing Hanzhou Innovation Institute Yuhang, Xixi Octagon City, Yuhang District, Hangzhou 310023, China.

[e]also at: Department of Environmental Sciences, Faculty of Meteorology, Environment and Arid Land Agriculture, King Abdulaziz University, Jeddah, Saudi Arabia.

**Correspondence to: D.E.Heard@leeds.ac.uk, L.K.Whalley@leeds.ac.uk*

Abstract The impact of heterogeneous uptake of HO_2 onto aerosol surfaces on radical concentrations and the O_3 production regime in Beijing summertime was investigated. The uptake coefficient of HO_2 onto aerosol surfaces, γ_{HO_2}, was calculated for the AIRPRO campaign in Beijing, Summer 2017, as a function of measured aerosol soluble copper concentration, $[Cu^{2+}]_{eff}$, aerosol liquid water content, [ALWC], and particulate matter concentration, [PM]. An average γ_{HO_2} across the entire campaign of 0.070 ± 0.035 was calculated, with values ranging from 0.002 to 0.15, and found to be significantly lower than the value of γ_{HO_2} = 0.2, commonly used in modelling studies. Using the calculated γ_{HO_2} values for the Summer AIRPRO campaign, OH, HO_2 and RO_2 radical concentrations were modelled using a box-model incorporating the Master Chemical Mechanism (v3.3.1), with and without the addition of γ_{HO_2}, and compared to the measured radical concentrations. Rate of destruction analysis showed the dominant HO_2 loss pathway to be HO_2 + NO for all NO concentrations across the Summer Beijing campaign with HO_2 uptake contributing < 0.3 % to the total loss of HO_2 on average. This result for Beijing summertime would suggest that under most conditions encountered, HO_2 uptake onto aerosol surfaces is not important to consider when investigating increasing O_3 production with decreasing [PM] across the North China Plain. At low [NO], however, i.e. < 0.1 ppb, which was often encountered in the afternoons, up to 29% of modelled HO_2 loss was due to HO_2 uptake on aerosols when calculated γ_{HO_2} was included, even with the much lower γ_{HO_2} values compared to γ_{HO_2} = 0.2, a results which agrees with the aerosol-inhibited O_3 regime recently proposed by Ivatt et al., 2022. As such it can be concluded that in cleaner environments, away from polluted urban centres where HO_2 loss chemistry is not dominated by NO but where aerosol surface area is high still, changes in PM concentration and hence aerosol surface area could still have a significant effect on both overall HO_2 concentration and the O_3 production regime.

Using modelled radical concentrations, the absolute O_3 sensitivity to NO_x and VOC showed that, on average across the summer AIRPRO campaign, the O_3 production regime remained VOC-limited, with the exception of a few days in the afternoon when the NO mixing ratio dropped low enough for the O_3 regime to shift towards NO_x-limited. The O_3 sensitivity to VOC, the dominant regime during the summer AIRPRO campaign, was observed to decrease and shift towards a NO_x sensitive regime both when NO mixing ratio decreased and with the addition of aerosol uptake. This suggests that if $[NO_x]$ continues to decrease in the future, ozone reduction policies focussing solely on NO_x reductions may not be as efficient as expected if

[PM] and, hence, HO_2 uptake to aerosol surfaces, continues to decrease. The addition of aerosol uptake into the model, for both the γ_{HO_2} calculated from measured data and when using a fixed value of γ_{HO_2} = 0.2, did not have a significant effect on the overall O_3 production regime across the campaign. While not important for this campaign, aerosol uptake could be important for areas of lower NO concentration that are already in a NO_x-sensitive regime.

1 Introduction

Climate change and air quality are two significant environmental issues faced by society today with the drive to net zero emissions by 2050 becoming increasingly important to remain consistent with the long-term anthropogenic temperature warming outcome of below 1.5 ºC as set out by the Paris Agreement in 2016. Increasing anthropogenic emissions have caused not only an increase in atmospheric warming, but also a deterioration in atmospheric air quality: a concern due to both short and long term negative health effects seen as a product of poor air quality such as respiratory and cardiovascular diseases and cancer (Brauer et al., 2016; Gakidou et al., 2017), in addition to a variety of negative effects on the environment such as increased soil acidification and the ensuing damage to vegetation and crop yield as a by-product of increasing acidity of rain (Forster et al., 2007).

Ambient air pollution has become a serious issue globally, specifically in large urban areas effected by anthropogenic emission sources. Due to rapid industrialisation, Chinese megacities in particular face significant environmental and health challenges from the decline in air quality following urbanisation, with areas such as the Beijing-Tianjin-Hebei area in the North China Plain (NCP) suffering from seasonal extreme pollution episodes as a consequence (Wang, 2021; Jin et al., 2016). In terms of human health, the most important pollutants in many regions are ground level O_3, NO_x (NO_2 and NO) and particulate matter. Nitrogen dioxide (NO_2) can be directly emitted into the atmosphere from high temperature combustion sources or can be formed via the reaction of nitrogen monoxide (NO) with an oxidising species in the troposphere, such as HO_2, leading to the formation of hydroxyl radical (OH) (Ye et al., 2017). Ozone, while vital in the stratosphere to protect the earth from harmful UV radiation and excessive planetary heating, is toxic to both plant and human life at ground level and can react with NO to form NO_2. Particulate matter is emitted anthropogenically and biogenically and can play a role in the warming and cooling of the atmosphere due to the ability of aerosols to absorb or scatter IR radiation depending on their composition. High levels of particulate matter, NO_x

and tropospheric O_3 in areas of low atmospheric mixing lead to photochemical smog and the reduction of visibility characteristic of extreme pollution episodes.

The concentration of pollutants and trace gases in the troposphere is controlled not only by emission levels but also by the oxidation capacity of the atmosphere which is determined largely by the concentration of the hydroxyl radical (OH) and the closely coupled hydroperoxyl (HO_2) radical, referred to collectively as HO_x radicals. Known for their role in chemical oxidation processes in the atmosphere, OH and HO_2 are vital species when considering climate change and air pollution. The OH radical is the main daytime tropospheric oxidant, with a major role as a source of ground level ozone (O_3) (Levy, 1971) and as a sink for both atmospheric pollutants, such as methane, and other radical species. The OH radical also has a role in the formation of secondary pollutants including secondary organic aerosols (SOAs) formed via the oxidation of volatile organic compounds (VOCs). OH and HO_2 radicals are closely linked, due to the recycling of HO_2 to give OH, either via the reaction with NO or CO, with the dominant loss pathway of HO_2 in polluted regions being the reaction with NO to form OH (for example, as shown in Beijing by Slater et al., 2020; Whalley et al., 2021). As such, understanding the sources and sinks of both OH and HO_2 within the troposphere is crucial to fully understand the concentration and distribution of trace atmospheric species associated with climate change and poor air quality.

Observed HO_2 concentrations from field measurements frequently can-not be fully explained by atmospheric chemistry models which often have a tendency to over-predict HO_2 in low NO_x conditions (Kanaya et al., 2007; Commane et al., 2010; Whalley et al., 2010; Whalley et al., 2021; Slater et al., 2020; Sommariva et al., 2004). Following the ClearfLo campaign in London 2012, zero-dimensional modelling showed an over-prediction of HO_2 by up to a factor of 10 at low NO_x which was attributed to uncertainties in the degradation mechanism of complex biogenic and diesel-related VOC species at low NO_x (Whalley et al., 2018). Over-prediction of HO_2 is also commonly thought to be due, in part, to lack of understanding of HO_2 uptake onto aerosol surfaces. A 2014 modelling study by Xue et al., 2014 focussing on the transport, heterogeneous chemistry and precursors of ground level ozone in Beijing, Shanghai, Guangzhou and Lanzhou, identified HO_2 uptake as a source of uncertainty when considering ozone production, with uptake onto aerosols having the largest effect on HO_2 concentration in Beijing where aerosol loadings were the highest.

While the impact of HO_2 uptake on HO_x concentrations has been calculated to vary from ~10-40 % (Jacob, 2000; Whalley et al., 2010; Whalley et al., 2021; Slater et al., 2020; Mao et al., 2010; Li et al., 2019; Li et al., 2018) globally, often a single value of γ_{HO_2}= 0.2 is used within models, as recommended by Jacob, 2000. Previous experimental studies report uptake coefficients which span several orders of magnitude, however, and vary largely based on the state of the aerosol and whether transition metal ion catalysis is involved. For dry inorganic salt aerosols values as low as γ_{HO_2} < 0.002 have been reported (Cooper and Abbatt, 1996; Taketani et al., 2008; George et al., 2013) increasing to up to γ_{HO_2}= 0.2 for aqueous aerosols (Thornton and Abbatt, 2005; Taketani et al., 2008; George et al., 2013). Previous experimental studies report much higher γ_{HO_2}> 0.4 for Cu-dopped aqueous aerosols (Thornton and Abbatt, 2005; Mozurkewich et al., 1987; Taketani et al., 2008; George et al., 2013; Lakey et al., 2016). Recently, larger values of γ_{HO_2} have been measured experimentally from samples taken offline at Mt. Tai (0.13-0.34) and Mt. Mang (0.09-0.40) in China by Taketani et al., 2012, while another study in Kyoto, Japan, directly measured γ_{HO_2} values under ambient conditions from 0.08 to 0.36 (Zhou et al., 2020). With γ_{HO_2} > 0.1, HO_2 concentrations can be significantly influenced particularly in areas of low [NO] and/or high aerosol loadings (Lakey et al., 2015; Matthews et al., 2014; Mao et al., 2013; Zhou et al., 2021; Martinez et al., 2003).

Following multiple policies implemented across China in response to the poor air quality "crisis", a number of studies have reported a decrease in NO_x and $PM_{2.5}$ emissions in China (Jin et al., 2016). Liu et al., 2017 reported NO_x (NO_2 + NO) emissions over 48 Chinese cities to have decreased by 21 % in the period of 2011-2015, supported by observed declines in NO_x emissions reported by other studies (Krotkov et al., 2016; Liu et al., 2016; Miyazaki et al., 2017; Van Der A et al., 2017). Ma et al., 2016b reported a mean annual decrease in $PM_{2.5}$ of 0.46 μg m^{-3} between 2008-2013, while Lin et al., 2018 reported an average decrease of 0.65 μg m^{-3} yr^{-1} between 2006-2010 increasing to a decline of 2.33 μg m^{-3} yr^{-1} for the period of 2011-2015. In contrast to the observed decrease in NO_x and $PM_{2.5}$ emissions, several studies have reported increasing O_3 levels. Ma et al., 2016a reported a maximum daily average 8h mean (MDA8) increase in O_3 concentrations of 1.13 ppb yr^{-1} for the period between 2003-2015 at a rural site north of Beijing while satellite observations suggested ground level ozone had increased ~7% for the period between 2005-2010 (Verstraeten et al., 2015). A recent study by Silver et al., 2018 also observed a significant increase in O_3 concentrations with median MDA8 increasing at a rate of 4.6 μg m^{-3} yr^{-1} across China.

A 2018 modelling study using the regional model GEOS-Chem by Li et al., 2018 suggested the increase in O_3 across China between 2013-2017 could be attributed to the decrease in $PM_{2.5}$, with changes in $PM_{2.5}$ being a more important driver of increasing O_3 trends than NO_x and VOC emissions for the period studied. It was proposed that a decrease in $PM_{2.5}$ emissions had led to a decrease in loss of HO_2 via aerosol uptake resulting in an increase in HO_2 concentration, and a proportional increase in the loss of HO_2 via NO leading to NO_2 which, when photolyzed, forms O_3 leading to an increase in O_3 (Li et al., 2018). However, analysis of measured radical budget from a field campaign in the North China Plain in Summer 2014 with a calculated γ_{HO_2} of 0.08 ± 0.13, showed no evidence for a significant impact of HO_2 heterogeneous chemistry on radical concentrations in North China Plain, concluding that reduced HO_2 uptake was unlikely to therefore be the cause of increasing O_3 levels in the North China Plain (Tan et al., 2020). Using a novel parameterisation developed by Song et al., 2020 in the framework of the resistor model to take into account the influence of aerosol soluble copper, aerosol liquid water content and particulate matter concentration on HO_2 uptake, and the Multiphase Chemical Kinetic box model (PKU-MARK) to assess the impact of HO_2 uptake on the O_3 budget for Wangdu Campaign in 2014, Song et al., 2022 concluded that HO_2 heterogeneous processes could decrease the O_3 production rates by up to 6 ppbv hr^{-1}, particularly in the morning VOC-limited regime.

In this study, the new parameterisation introduced by Song et al., 2021, hereafter referred to solely as the Song parameterisation, coupled with measured data from the Summer AIRPRO campaign in Beijing 2017 was used to calculate a time series of the HO_2 uptake coefficient, which was then used to investigate the impact of heterogeneous uptake of HO_2 onto aerosol surfaces on the HO_2 radical budget in Summertime Beijing using the Master Chemical Mechanism and the impact on the O_3 regime. We will test the hypothesis that reduced HO_2 uptake due to a reduction in $PM_{2.5}$ concentration is a significant driver of the recent increase in ozone concentrations in China.

2 Experimental

2.1 Campaign overview and site description

As part of the Atmospheric Pollution and Human Health (APHH) in a Chinese Megacity programme, the University of Leeds took simultaneous measurements of OH, HO_2, RO_2 and OH reactivity (k_{OH}), in addition to measurements of HCHO and photolysis rates, during two

field campaigns at an urban site in Winter 2016 and Summer 2017 in Beijing, with the aim to study the chemical and physical processes governing gas and particle pollution and meteorological dynamics in the Beijing region and the links between the two (Shi et al., 2019; Slater et al., 2020; Whalley et al., 2021). The two field campaigns in Beijing were part of the AIRPRO (The integrated study of AIR pollution PROcesses in Beijing) project within the APHH programme, described fully by Shi et al., 2019.

For the summer AIRPRO campaign, the official science period was from 23rd May 2017 to the 22nd June 2017, with observations taking place at the Institute of Atmospheric Physics (IAP) within the Chinese Academy of Sciences, located between the third and fourth ring roads in central Beijing within 100 m of a major road, making local traffic emission sources an important source of pollution during measurement period. All instrumentation for the campaign was located at this site, housed within nine shipping containers surrounding a meteorological tower. Further details of the instrumentation and measurement site can be found in Shi et al., 2019. A detailed description of the University of Leeds Fluorescence Assay by Gas Expansion (FAGE) instrument used to make the measurements of OH, HO_2 and RO_2 radicals discussed in further sections can be found in Section 1.1 of Supplementary Information.

2.2 Determination of aerosol soluble copper concentration through ICP-MS Analysis

The soluble copper ion concentration was determined by analysing the effluent extracted from quartz filter samples taken daily for the entire campaign using Inductively Coupled Plasma Mass Spectrometry (ICP-MS). A 6 cm^2 punch from each large quartz filter $PM_{2.5}$ sample was cut and put in a 15 mL extraction tube and extracted with 10 mL ultrapure water (18.2 MΩ cm) under ultrasonication for 60 minutes at below 35 ^oC. The sample was then shaken by a temperature-controlled shaker at 4 ^oC for 3 hours at approximately 60 cycles min^{-1}. After filtering through a filter syringe, 8 mL of effluent was transferred to a new 15 mL metal free tube, and 2 mL of 10% HNO_3 was added to make a 10 mL 2% HNO_3 extract solution which was then analysed to determine the soluble copper ion concentration using ICP-MS.

2.3 MCM v3.3.1 box model description

The Master Chemical Mechanism (MCM*v*3.3.1) is a near-explicit mechanism which describes the gas-phase degradation of a series of primary emitted VOC's in the troposphere. The

mechanism considers the degradation of 143 VOC's and contains ~17000 elementary reactions of 6700 species (Whalley et al., 2013).

The model was constrained to measurements of NO, NO_2, O_3, CO, HCHO, HNO_3, HONO, PAN, H_2O vapour, temperature, pressure, $j(O^1D)$, j(HONO), $j(NO_2)$, $j(ClNO_2)$, j(HOCl), $j(ClONO_2)$ and specific VOC species measured using GC-FID (gas chromatography with flame ionisation) and PTR-ToF-MS (proton-transfer reaction time of flight mass spectrometry). The measured species were input into the model at a time resolution of 15 minutes, with species measured at a higher time resolution averaged up to 15 minutes and those measured at a lower time resolution interpolated to give a value every 15 minutes. The full list of all species constrained in the model is shown in Table 1.

Type	Species
Gas-phase inorganic species	NO, NO_2, O_3, CO, HNO_3, HONO, H_2O, SO_2, $ClNO_2$, HOCl
Gas-phase organic species	HCHO, PAN, CH_4, C_2H_6, C_2H_4, C_3H_8, C_3H_6, isobutane, butane, C_2H_2, trans-but-2-ene, but-1ene, Isobutene, cis-but-2-ene, 2-Methylbutane, pentane, acetone, 1,3-butadiene, trans-2-pentene, cis-2- pentene, 2-methylpetane, 3-methypetane, hexane, isoprene, heptane, benzene, toluene, nonane, decane, undecane, dodecane, o-xylene, CH_3OH, CH_3OCH_3, 2-ethyltoluene, 3-ethyltoluene, 4-ethyltoluene, ethylbenzene, CH_3CHO, C_2H_5OH, α-pinene, limonene, isopropylbenzene, propylbenzene, m-xylene, p-xylene, 1,2,3-trimethylbenzene, 1,2,4-trimethylbenzene, 1,3,5-trimethylbenzene.
Photolysis rates	$j(O^1D)$, j(HONO), $j(NO_2)$, $j(ClNO_2)$, j(HOCl), $j(ClONO_2)$
Other	Mixing height, aerosol surface area

Table 1. Full description of measured species during Summer AIRPRO campaign constrained within the model

The different model scenarios referred to in this study are described in full below:

1. **MCM_base:** The base model run constrained to species described in Table 1.
2. **MCM_gamma:** The base model including heterogeneous HO_2 uptake onto aerosols with γ_{HO_2} calculated from parameterisation developed by Song et al., 2020.
3. **MCM_SA:** The base model including heterogeneous HO_2 uptake, this time with γ_{HO_2} fixed at 0.2, as commonly used within models and recommended by Jacob, 2000.

2.4 Calculation of L_N/Q and absolute O_3 sensitivity

First introduced by Kleinman et al., 1997, L_N/Q is the ratio of radical loss via NO_x to total primary radical production and is used as a means of determining O_3 production sensitivity to VOCs and NO_x (Kleinman, 2000; Kleinman et al., 1997; Kleinman et al., 2001). This method was then built on by Sakamoto et al., 2019 who included loss of peroxy radicals (XO_2=HO_2+RO_2) onto aerosol surfaces within the calculation of O_3 sensitivity.

The only source of tropospheric O_3 is by the reaction of peroxy radicals with NO, while the main source of XO_2 species is via the reaction of OH with VOCs.

$$XO_2 + NO \rightarrow XO + NO_2 \quad \text{(R 1)}$$

$$OH + VOC + O_2 \rightarrow XO_2 + products \quad \text{(R 2)}$$

The O_3 production rate in the troposphere is therefore:

$$P(O_3) = k_{HO_2+NO}[HO_2][NO] + k_{RO_2+NO}[RO_2][NO] \quad (1)$$

where k_{HO_2+NO} and k_{RO_2+NO} are the bimolecular rate constants for the reaction of HO_2 and RO_2 with NO.

The production rate of OH, HO_2 and RO_2 radicals, Q, must equal the loss rate:

$$Q = L_P + L_N + L_R \quad (2)$$

where L_P is the loss rate of radicals onto aerosol particles, L_N is the loss rate of radicals via reaction with NO_x species and $L_R$is the loss rate of radicals via radical-radical reactions to give peroxides.

$$L_P = k_{HO_2\ uptake}[HO_2] + k_{RO_2\ uptake}[RO_2] = k_P[XO_2] \quad (3)$$

$$L_N \approx k_{NO_2+OH}[NO_2][OH] \quad (4)$$

$$L_R = 2(k_{HO_2+HO_2}[HO_2]^2 + k_{RO_2+HO_2}[HO_2][RO_2]) \quad (5)$$

where $k_{HO_2\ uptake}$ is the rate constant for the loss of HO_2 onto aerosol surfaces, $k_{RO_2\ uptake}$ is the rate constant for the loss of RO_2 onto aerosol surfaces, k_{NO_2+OH} is the bimolecular rate constant for the reaction of NO_2 with OH, $k_{HO_2+HO_2}$is the bimolecular rate constant for the self-reaction of HO_2 and $k_{RO_2+HO_2}$is the bimolecular rate constant for the reaction of RO_2 with HO_2.

For radical loss onto aerosol surfaces, the rate constant is given as a function of the reactive uptake coefficient, γ_{XO_2}, aerosol particle surface area ($cm^2\ cm^{-3}$) and mean thermal velocity

(cm s^{-1}), given by $\nu = \sqrt{8RT/\pi M}$ with R, T and M as the gas constant, the absolute temperature and the molar mass of species respectively.

$$k_{radical\ uptake} = \frac{\gamma_{XO_2} \times SA \times \nu}{4} \quad (6)$$

According to the method described in Sakamoto et al., 2019, the ratio of radical loss to NO_x to primary O_3 production including radical loss via aerosol uptake, $\frac{L_N}{Q}$ is defined as follows:

$$\frac{L_N}{Q} = \frac{1}{1 + \left(\frac{(2k_R[XO_2] + k_P)k_{OH+VOC}[VOC]}{(1-\alpha)k_{HO_2+NO}[NO]k_{NO_2+OH}[NO_2]}\right)} \quad (7)$$

where k_{OH+VOC} is the bimolecular rate constant for the loss of OH via reaction with VOCs and $(1-\alpha)$ is the fraction of XO_2 that is HO_2.

The relative sensitivity of O_3 production to NO_x and VOCs is described by:

$$\frac{\delta lnP(O_3)}{\delta \ln [NO_x]} = (1-\chi)\left(\frac{1 - \frac{3}{2}\frac{L_N}{Q}}{1 - \frac{1}{2}\frac{L_N}{Q}}\right) + \chi(1 - 2\frac{L_N}{Q}) \quad (8)$$

$$\frac{\delta lnP(O_3)}{\delta \ln [VOC]} = (1-\chi)\left(\frac{\frac{1}{2}\frac{L_N}{Q}}{1 - \frac{1}{2}\frac{L_N}{Q}}\right) + \chi\frac{L_N}{Q} \quad (9)$$

where $\chi = \frac{L_P}{L_P + L_R}$. The O_3 regime transition point, where $\frac{\delta lnP(O_3)}{\delta \ln [NO_x]} = \frac{\delta lnP(O_3)}{\delta \ln [VOC]}$, is given by $\frac{L_N}{Q_{trans}}$.

$$\frac{L_N}{Q_{trans}} = \frac{1}{2}(1-\chi) + \frac{1}{3}\chi \quad (10)$$

Absolute O_3 sensitivity was introduced by Sakamoto et al., 2019, and allows for the assessment of how reduction in O_3 precursors could contribute to reduction in $P(O_3)$ by integrating over time and area. The absolute sensitivity of O_3 production to VOC and NO_x is then described by:

$$Absolute\ P(O_3) = \frac{\delta P(O_3)}{\delta \ln [X]} = P(O_3)\frac{\delta P(O_3)}{\delta \ln [X]} \quad (11)$$

where is *[X]* is NO_x or VOC.

2.5 Description of the "Song parameterisation"

A large uncertainty in determining the effect of HO_2 uptake onto the surface of aerosol particles is the lack of understanding of the dependence of γ_{HO_2} on Cu (II)/transition metal ion

concentration within aerosols. Experimentally this dependence is quite well known from laboratory studies (Mozurkewich et al., 1987; Thornton and Abbatt, 2005; George et al., 2013; Mao et al., 2013), however the effective concentrations in ambient aerosols and the impact on γ_{HO_2} of aerosol liquid water concentration, [ALWC], has not been incorporated into models before. A novel parameterisation was developed by Song et al., 2020 in the framework of the resistor model to include the influence of aerosol soluble copper on the uptake of HO_2. The new parameterisation for the uptake coefficient of HO_2 onto aerosols, as given in Song et al., 2020, is as follows:

$$\frac{1}{\gamma_{HO_2}} = \frac{1}{\alpha_{HO_2}} + \frac{3 \times \nu_{HO_2}}{(4 \times 10^6) \times R_d H_{eff} RT \times \left(5.87 + 3.2 ln\left(\frac{ALWC}{[PM] + 0.067}\right)\right) \times [PM]^{-0.2} \times [Cu^{2+}]_{eff}^{0.65}} \quad (12)$$

where γ_{HO_2} is the uptake coefficient of HO_2 onto aerosols, α_{HO_2} is the mass accommodation coefficient of HO_2, ν_{HO_2} is the mean molecular speed in cm s^{-1}, R_d is the count median radius of the aerosol in cm, H_{eff} is the effective Henry's Law constant calculated from $H_{eff} = H_{HO_2}\left(1 + \frac{K_{eq}}{[H+\}}\right)$ where H_{HO_2} is the physical Henry's Law constant for HO_2 (i.e. 3900 (Thornton et al., 2008)) in M atm^{-1}, K_{eq} is the equilibrium constant for HO_2 dissociation (M), and $[H^+]$ is the hydrogen ion concentration within the aerosol calculated from the pH (M), R is the gas constant in cm^3 atm K^{-1} mol^{-1} (i.e. 82.05), T is the temperature in K, $[ALWC]$ is the aerosol liquid water content in µg m^{-3} (which is related to the ambient relative humidity), $[PM]$ is the mass concentration of $PM_{2.5}$ in µg m^{-3} and $[Cu^{2+}]_{eff}$ is the effective aerosol condensed-phase soluble copper (II) ion concentration in mol L^{-1}.

The Song parameterisation can reportedly be used for urban environmental conditions of aerosol mass concentrations between 10-300 µg m^{-3}; aqueous copper (II) concentrations of 10^{-5}–1 mol L^{-1}; and relative humidity between 40-90 %. However, for the Summer AIRPRO campaign data, the minimum [ALWC] supported by the parameterisation was 14 µg m^{-3}, below which the parameterisation returned negative values for γ_{HO_2}. As such, despite the average calculated [ALWC] for the campaign being 6.9 ± 10 µg m^{-3}, a fixed value of 14 µg m^{-3} was used to calculate γ_{HO_2} across the entire campaign.

3 Results and Discussion

3.1 Overview of field observations during summer AIRPRO campaign

Radical concentration measurements were taken throughout the official science period of the summer campaign, from 23/05/2017 to 22/06/2017, using the Fluorescence Assay by Gas Expansion technique. Alongside the radical observations and photolysis rate measurements made by the University of Leeds, there was a varied suite of supporting measurements operated by several universities and institutions. The supporting measurements used for the analysis and discussion in this study were provided chiefly by the Universities of York, Birmingham and Cambridge as detailed in Table 2.

Instrument	Species measured	University	Reference
FAGE	OH, HO_2, RO_2	Leeds	Whalley et al., 2010; Whalley et al., 2021; Slater et al., 2020
OH reactivity	OH reactivity	Leeds	Stone et al., 2016; Whalley et al., 2021; Slater et al., 2020
Spectral Radiometer	Photolysis rates	Leeds	Bohn et al., 2016
Filter Radiometer	$j(O^1D)$	Leeds	Whalley et al., 2010
Teledyne CAPS	NO_2	York	Smith et al., 2017
TEI 42c	Total NO_y	York	Smith et al., 2017
TEI 49i	O_3	York	Smith et al., 2017
Sensor box	CO	York	Smith et al., 2017
DC-GC_FID	C_2-C_7 VOCs and oVOCs	York	Hopkins et al., 2011
GCxGC-FID	C_6-C_{13} VOCs and oVOCs	York	Dunmore et al., 2015
BBCEAS	HONO	Cambridge	Le Breton et al., 2014
TEI 42i	NO	Birmingham	-
LOPAP	HONO	Birmingham	Crilley et al., 2016
SMPS	Particle Size distribution	Birmingham	Wiedensohler et al., 2012
High volume sampler	$PM_{2.5}$ filter samples, Aerosol copper	IAP	-

Table 2. Measurements taken by universities and institutions during the Beijing Summer AIRPRO campaign. These species are directly referred to in this chapter: full description of every instrument and measurement taken can be found in Slater, 2020. IAP: Institute of Atmospheric Physics, Beijing. Time resolution of all instruments was averaged up to or interpolated down to 15 minutes for modelling purposes with the exception of the $PM_{2.5}$ filter samples, of which there was only 1 sample taken a day.

The median average diurnals for important gas phase species (ppb) and $j(O^1D)$ (s^{-1}) measured during the summer campaign are shown in Figure 1. $j(O^1D)$ showed a maximum at solar noon peaking at 2.5×10^{-5} s^{-1}. The diurnal variation in both NO and NO_2 was very distinct, with a peak in NO at rush hour (~08:00) of ~ 8 ppb. NO decreased into the afternoon following this morning peak to a minimum of 0.3 ppb. The low values of NO mixing ratio observed in the afternoon were a result of high levels of O_3, peaking at 89 ppb at ~15:30, leading to increased titration of NO + O_3 to give NO_2, the diurnal of which can be seen to peak in the morning at ~ 32 ppb at 06:30, coinciding with peak in traffic emissions. Conversely O_3 mixing ratio was at a minimum of ~14 ppb during the morning traffic peak in NO. Due to the expected

accumulation of HONO overnight, HONO mixing ratio is highest in the morning, peaking before 07:30 at ~ 7 ppb, after which HONO is lost rapidly via photolysis to give OH + NO. This study will use these measured observations to compare modelled and measured concentrations of OH, HO_2 and RO_2 radicals and investigate the effect of HO_2 uptake on radical concentrations.

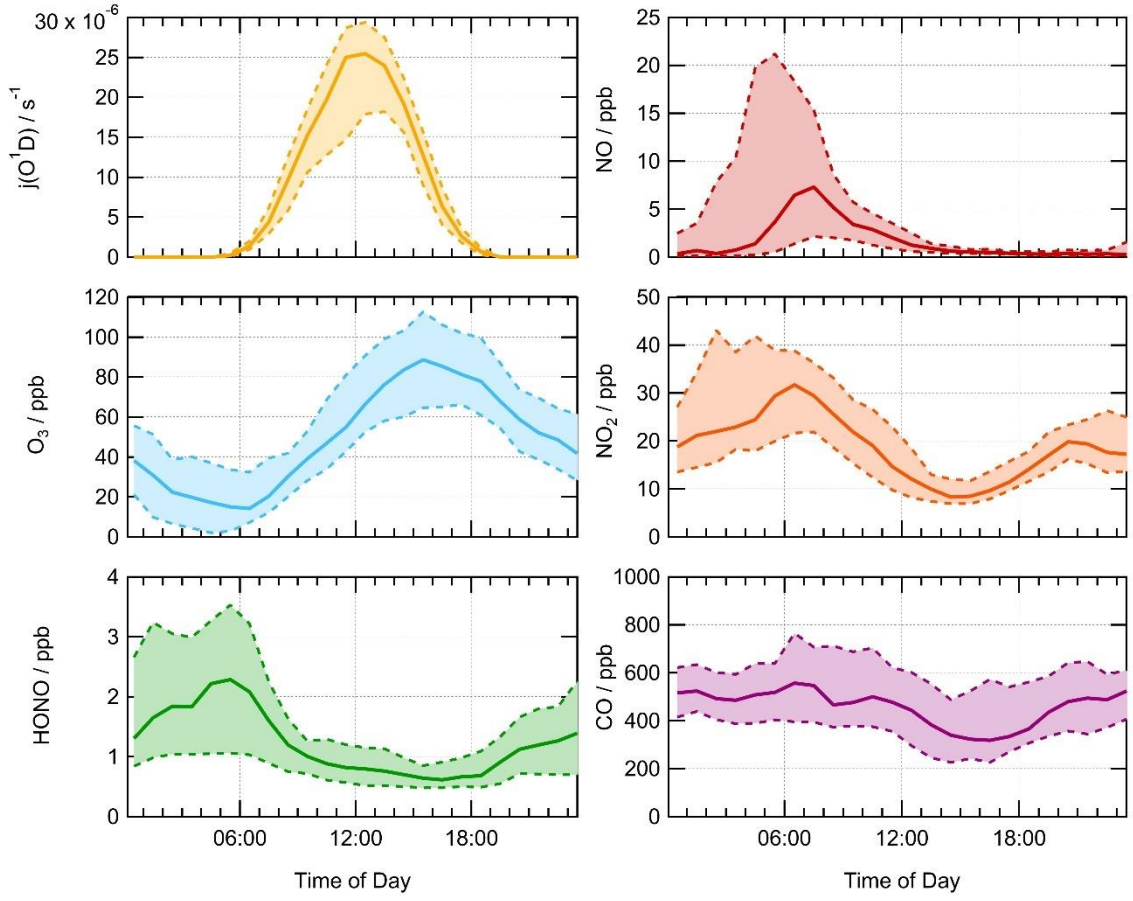

Figure 1. Average median diurnal profile for measured $j(O^1D)$ (s^{-1}), O_3 (ppb), HONO (ppb), NO (ppb), NO_2 (ppb) and CO (ppb) for the Summer AIRPRO campaign. The dashed lines with shaded regions represent the $25^{th}/75^{th}$ percentiles. Diurnals show 60 minute averages, taken over the entire measurement period.

The majority of the Summer Beijing campaign occurred during a non-haze period, meaning $PM_{2.5}$ concentrations remained below 75 µg m^{-3}, only exceeding this on the 28/05, 31/05, 05/06, 07/06, 17/06 and 18/06/2017. The average median diurnal of $PM_{2.5}$ surface area (cm^2 cm^{-3}) is shown in Figure 2. $PM_{2.5}$ surface area concentration was available at a higher resolution due to use of online particle sizers compared to filter samples taken daily to give $PM_{2.5}$ mass concentration. $PM_{2.5}$ surface area was then averaged up to a time resolution of 15 minutes to be used in the model. Online particle sizers were run without a drying inlet to ensure aerosol measurements were as close to real ambient size distributions as possible, and therefore

correction for hygroscopic growth was not necessary. No strong diurnal trend was seen, with an average across the campaign of 5.5 × 10^{-6} cm^2 cm^{-3}, with a maximum surface area of 2.5×10^{-5} cm^2 cm^{-3}.

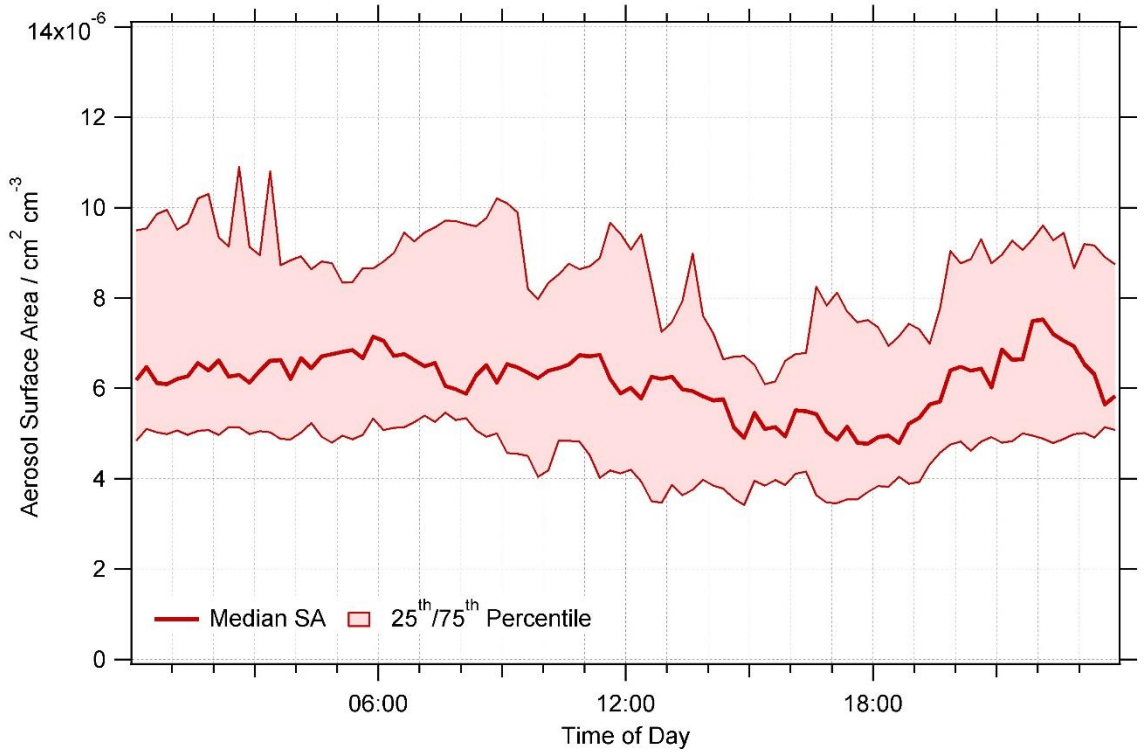

Figure 2. Average median diurnal of $PM_{2.5}$ aerosol surface area (cm^2 cm^{-3}) for Summer AIRPRO campaign. Data averaged up to 15 mins time resolution. The dashed lines with shaded regions represent the 25^{th}/75^{th} percentiles.

During haze periods in Beijing, it is expected that a strong correlation would exist between $PM_{2.5}$ and NO_x, as seen in Winter Beijing AIRPRO campaign in 2016 (Slater et al., 2020). However, during the Summer campaign, no strong correlation between $PM_{2.5}$ and NO_x was seen. The time series of NO (ppb) and $PM_{2.5}$ (cm^2 cm^{-3}) is shown in Figure 3. A correlation plot of $PM_{2.5}$ aerosol surface area (cm^2 cm^{-3}) versus NO and NO_2 mixing ratio (ppb) is shown in Figure 1 of Supplementary Information.

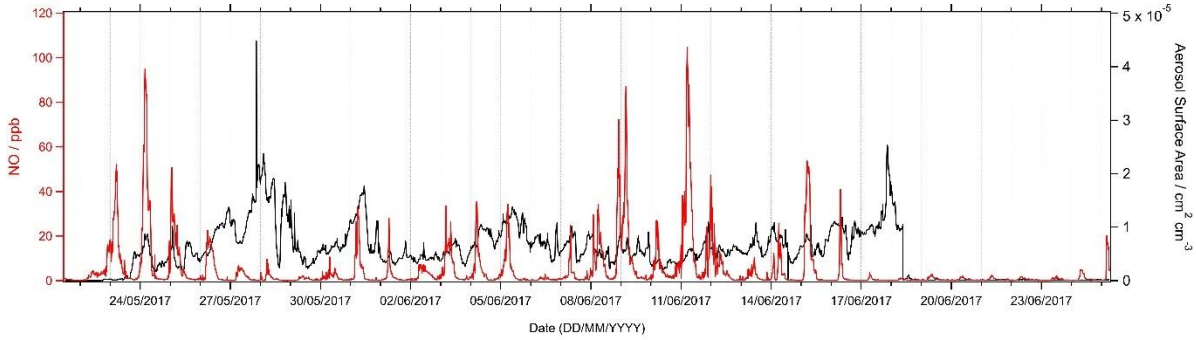

Figure 3. Time series of measured NO / ppb and $PM_{2.5}$ / $cm^2\,cm^{-3}$ across entire summer AIRPRO campaign in Beijing.

3.2 Calculated γ_{HO_2} for summer AIRPRO campaign

Measured values of [PM], copper (II) ion concentration and aerosol pH (used to calculate H_{eff} in equation 12), and values of [ALWC] estimated using the ISORROPIA-II thermodynamic equilibrium model (Fountoukis and Nenes, 2007) were input into the parameterisation at a time resolution of 1 day. $PM_{2.5}$ mass concentration and Cu (II) ion concentration values were measured by extracting from filter samples offline with one filter sample taken every day. As such all measured values input into the parameterisation were averaged up to this time resolution. R_d was calculated from the measured aerosol size distribution across the entire campaign. A value of 0.5 was chosen for the mass accommodation coefficient, a_{HO_2}, to reflect values previously measured for copper doped inorganic salts (Thornton and Abbatt, 2005; George et al., 2013; Taketani et al., 2008) and to allow better comparison with results from Song et al., 2020. For summer AIRPRO campaign, the soluble copper ion concentration was measured by extracting Cu (II) ions from filter samples and analysing the effluent using Inductively Coupled Plasma Mass Spectrometry (ICP-MS). As in Song et al., 2020, the total copper (II) mass concentration (ng m^{-3} converted to g m^{-3}) was divided by the aerosol volume concentration (nm^3 cm^{-3} converted to dm^3 m^{-3}) and the molar mass of copper (g mol^{-1}) to give the total copper molar concentration in the aerosol, $[Cu^{2+}]_{eff}$ (mol L^{-1}), which was then used in equation 12. The average values across summer AIRPRO campaign for parameters used in equation 12 are shown in Table 3.

Parameter	Average value across campaign
Temperature (K)	300
Relative humidity (%)	43
Aerosol pH	3
Count median radius (cm)	2.3×10^{-6}
ALWC (μg m^{-3})^{a}	14
[PM] (μg m^{-3})	38.3
[Cu^{2+}]$_{eff}$ (mol L^{-1})	0.0008
[Cu^{2+}]$_{eff}$ (ng m^{-3})	4
$\boldsymbol{a_{HO_2}}$	0.5 (fixed)

Table 3. Average values for summer AIRPRO campaign in Beijing, 2017 for parameters in equation 12. [a]This was a fixed minimum value of ALWC for the parameterisation to be used for this data set, fully explained in Section 3.4. Cu (II) ion concentration is given in both mol L^{-1} and ng m^{-3}, due to mol L^{-1} being used in equation 12 but ng m^{-3} being the more atmospherically relevant unit.

For the Beijing summer AIRPRO campaign, an average value of γ_{HO_2} = 0.07 ± 0.035 (1σ) was calculated across the entire campaign, with values ranging from 0.002 to 0.15. The time series for the calculated γ_{HO_2}, R_d (cm), [PM] (μg m^{-3}), [ALWC] (μg m^{-3}) and [Cu^{2+}]$_{eff}$ (mol L^{-1}) is shown in Figure 4.

As fully described in Song et al., 2020 supplementary information, the uncertainty in the calculation of γ_{HO_2} using equation 12 comes mainly from the uncertainty in [ALWC] (~10-20 %, calculated using ISORROPIA-II (Fountoukis and Nenes, 2007)), the uncertainty in the mass accommodation coefficient (varying a_{HO_2} within the parameterisation from 0.1 to 1, increased the calculated γ_{HO_2} from 0.042 to 0.077. However, by a_{HO_2} = 0.5 this dependence has begun to plateau with γ_{HO_2} = 0.070 when a_{HO_2}=0.5), and the uncertainty of the model calculations used to formulate the parameterisation (~40 % as explained in Song et al., 2020). Uncertainties in measured parameters i.e. temperature, [PM], [Cu^{2+}] and count median radius are due to associated instrumental error which are assumed small in comparison.

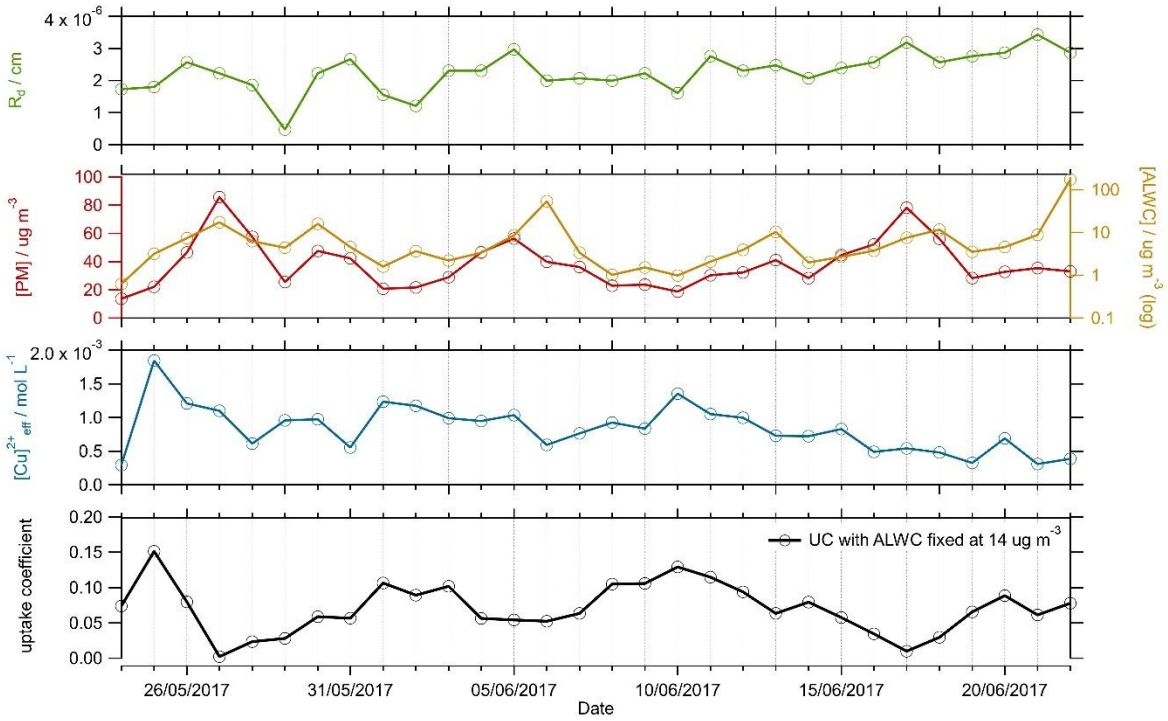

Figure 4. Time series of R_d (cm, orange), [PM] (μg m^{-3}, red), [ALWC] (μg m^{-3}, yellow) and $[Cu^{2+}]_{eff}$ (mol L^{-1}, blue), parameters used in equation 12 to calculate γ_{HO_2} (bottom panel). Each parameter has been averaged up to a time resolution of 1 day to match the lowest resolution measurement. The calculated γ_{HO_2} is shown in the bottom panel, for a fixed [ALWC] = 14 ug m^{-3} (solid black line).

To examine the effect within the Song parameterisation of [PM] and [ALWC] on γ_{HO_2} as a function of copper molarity, the uptake coefficient was calculated by varying the $[Cu^{2+}]_{eff}$ concentration within the parameterisation with alternatively fixed values of [PM] or [ALWC]. For a given value of $[Cu^{2+}]_{eff}$, at fixed [ALWC] an increase in [PM] causes a decrease in the curvature of γ_{HO_2} vs $[Cu^{2+}]_{eff}$, whereas at a fixed [PM], an increase in [ALWC] leads to an increase in γ_{HO_2} for a given $[Cu^{2+}]_{eff}$. As shown in Figure 5, [AWLC] and [PM] have the greatest effect on γ_{HO_2} between $[Cu^{2+}]_{eff}$= 10^{-5}-10^{-1}M before the curve levels off towards the mass accommodation coefficient of 0.5, as input into the model. For context within the Beijing campaign, the curve of γ_{HO_2}vs $[Cu^{2+}]_{eff}$ was plotted in Figure 5 using the average values for the AIRPRO summer campaign fixed at [ALWC] = 14 ug m^{-3} and [PM] = 38.3 ug m^{-3}. For the average AIRPRO summer campaign values, an increase $[Cu^{2+}]_{eff}$ has the most effect on γ_{HO_2} between $[Cu^{2+}]_{eff}$ ~10^{-3} -10^{-1} M, with the average $[Cu^{2+}]_{eff}$ for the campaign being 8 × 10^{-4} M (values ranged from 3 × 10^{-4} to 2 × 10^{-3} M across campaign).

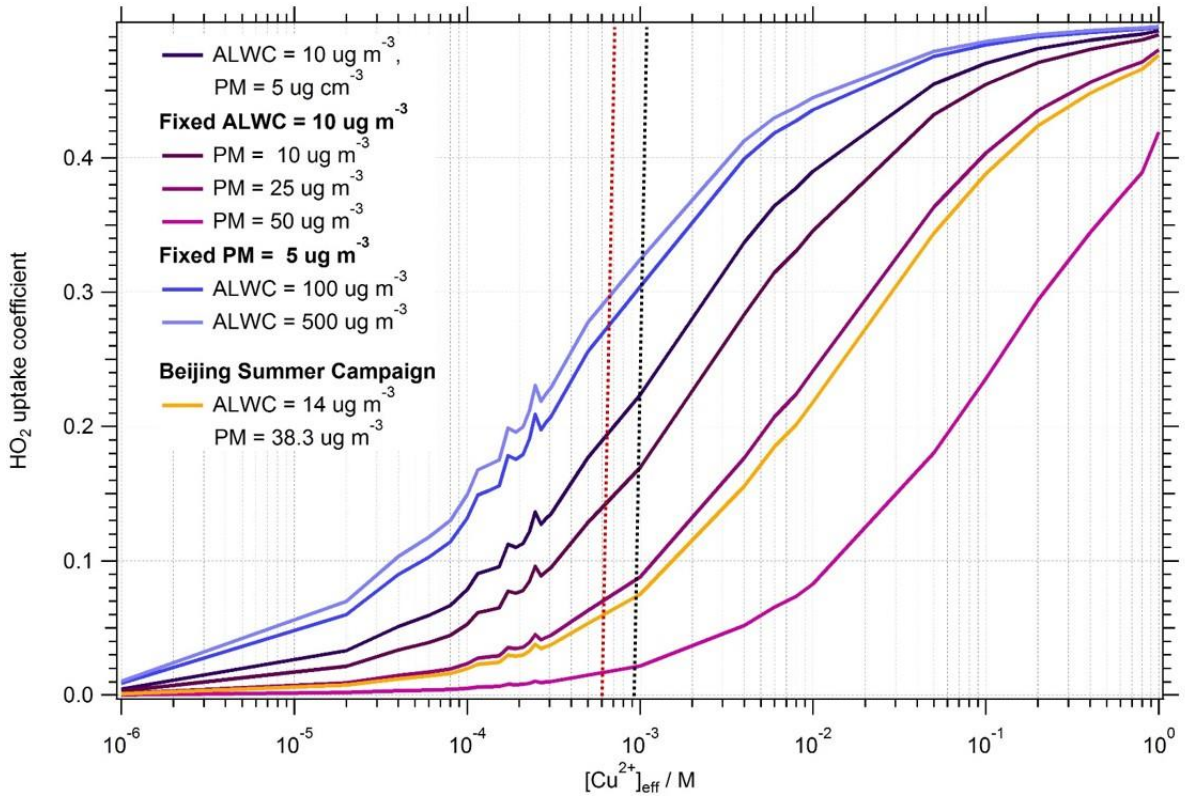

Figure 5. Dependence of uptake coefficient, γ_{HO_2} on aerosol copper concentration, $[Cu^{2+}]_{eff}$ (M), showing the effect of varying [PM] with fixed [ALWC] and vice versa. Pink to purple lines show the effect on uptake coefficient of varying [PM] from 5-50 µg m^{-3} with a fixed [ALWC] of 10 g cm^{-3}. Blue to dark blue lines show the effect on γ_{HO_2} of varying [ALWC] from 10-500 ug m^{-3} (much higher than typically seen atmospherically) with a fixed [PM] of 5 µg m^{-3}. The yellow line shows the effect on the γ_{HO_2} of varying $[Cu^{2+}]_{eff}$, with [ALWC] and [PM] taken as the averages from the Beijing campaign, i.e. [ALWC] = 14 ug m^{-3} and [PM] = 38.8 ug m^{-3}. Black dashed line indicates the average $[Cu^{2+}]_{eff}$ for Beijing summer campaign. Red dashed line indicates the average $[Cu^{2+}]_{eff}$ for the Wangdu campaign. Note that the [PM] and [ALWC] are both higher for Wangdu campaign compared to the Beijing campaign.

3.3 Box modelling results

3.3.1 Effect of calculated γ_{HO_2} on modelled AIRPRO Summer radical concentrations

As reported in Whalley et al., 2021, radical concentrations were high during the AIRPRO summer campaign with maximum measured concentrations of OH, HO_2 and RO_2 of 2.8×10^7 molecule cm^{-3}, 1×10^9 molecule cm^{-3} and 5.5×10^9 molecule cm^{-3} on the afternoons of the 30th May, 9th June and 15th June respectively. The time series of measured OH, HO_2 and RO_2 for the entire summer campaign as measured by the Leeds FAGE instrument with MCM_base model outputs for OH, HO_2 and RO_2 can be found in Whalley et al., 2021. Using the MCM and the γ_{HO_2} calculated for the Summer Beijing campaign with the Song parameterisation, the

effect of HO_2 uptake on the concentration of OH, HO_2 and RO_2 radicals was investigated and compared to the base model.

The MCM_base model predicted radical concentrations are shown as average diurnal profiles compared to both the measured diurnals and the MCM_gamma model in Figure 6. A detailed description of the diurnal variation in measured and modelled OH, HO_2 and RO_2 radicals for the summer Beijing campaign is given in Whalley et al., 2021, so only a brief summary will be given here.

The average diurnal profiles show that the MCM_base model can re-produce the measured OH concentrations relatively well, however the modelled peak in OH is shifted to the afternoon with a peak at ~14:00 compared to the midday peak in the observations. In comparison, HO_2 is over-predicted, particularly during the day with the exception being when NO was high from 9-12th June. Day-time HO_2 is over-predicted on average by MCM_base by up to a factor of ~2.9 with a peak in the diurnal at ~ 14:30. In-comparison, daytime RO_2 concentration is under-predicted on average by MCM_base by up to a factor of ~7.5, with a larger under-prediction in the morning between ~6:30-10:30 when NO levels were highest. At the peak of the RO_2 diurnal, on average the concentration was under-predicted by MCM_base by a factor of ~2.7. While the MCM_base model is able to reproduce measured OH concentrations reasonably well, the inability of this model to reproduce HO_2 and RO_2 suggests missing key reactions. In Whalley et al., 2021, budget analysis highlighted a missing source of OH, in addition to a missing RO_2 production reaction which could partially explain the under-prediction of RO_2 by the MCM_base model. It was also suggested that the over-prediction of HO_2 could be due, in part, to the propagation rate of RO_2 to HO_2 being significantly slower than currently included in the model. This could be due to a lack of understanding of the rate of reaction of RO_2 with NO to produce different RO_2 species, i.e. $RO_2 + NO \rightarrow RO_2$', which would lead to propagation of RO_2 to different, more oxidised RO_2 species, competing with the recycling of RO_2 via RO_2 to give HO_2. It is also possible, that the overestimation in the propagation rate of RO_2 to HO_2 could be due to a lack of RO_2 autoxidation pathways included within the model which could lead to the formation of highly oxygenated molecules as opposed to HO_2. The higher, measured RO_2 concentrations could, therefore, suggest that the lifetime of total RO_2 is longer than currently considered within the model.

As stated in Section 3.2, for the Beijing summer AIRPRO campaign, values of calculated γ_{HO_2} varied ranging from 0.002 to 0.15, giving an average value of γ_{HO_2}= 0.07 ± 0.035 (1σ) across

the campaign. These γ_{HO_2} values calculated on a daily time resolution, were added into the MCM_base model to give the MCM_gamma model. The average median diurnals of modelled OH, HO_2 and RO_2 (molecule cm^{-3}) for MCM_base, MCM_gamma (with γ_{HO_2} ranging from 0.002-0.15) and MCM_SA (with γ_{HO_2} fixed at 0.2) are shown in Figure 6.

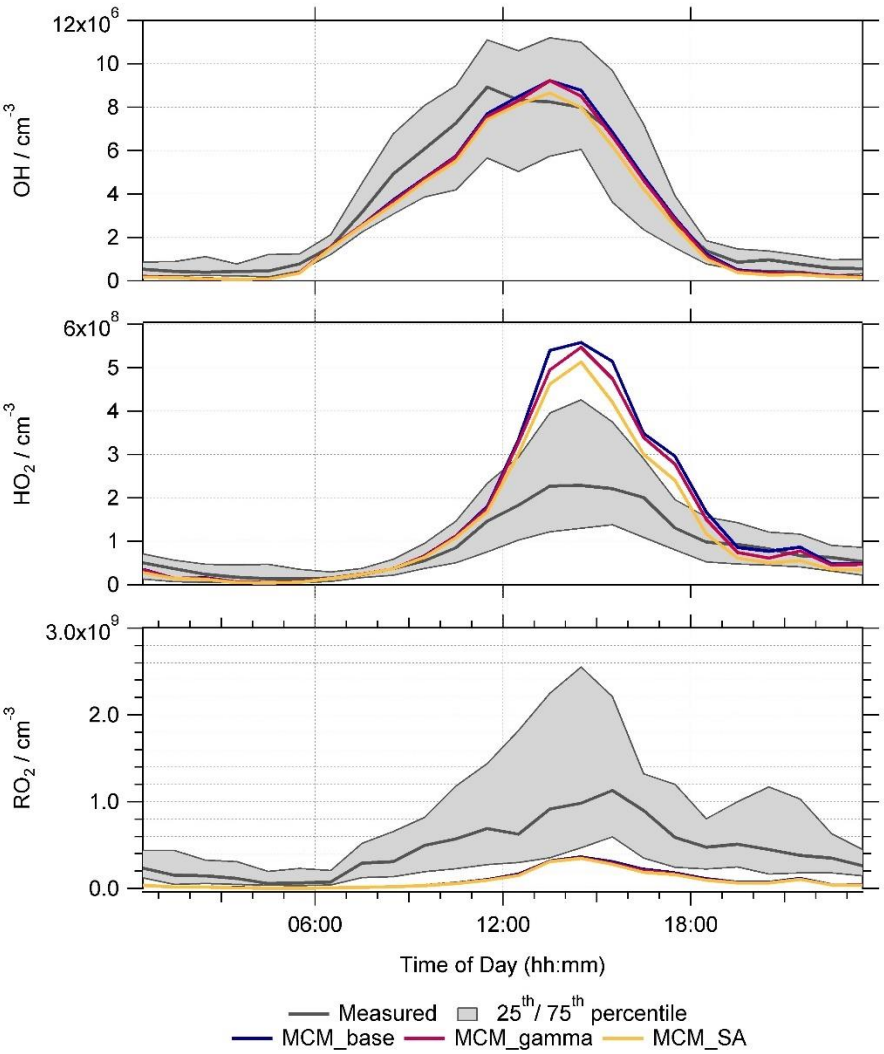

Figure 6. Average median diurnals for measured radical concentrations (grey) and modelled OH, HO_2 and total RO_2 radical concentrations in molecule cm^{-3} for MCM_base (blue), MCM_gamma (dark pink) and MCM_SA (yellow) model runs. All diurnal's are 60 minute averages, taken over the entire measurement period. Shaded grey regions represent the $25^{th}/75^{th}$ percentiles of measured radical data.

Due to a combination of the calculated uptake coefficient being smaller, on average, than usually used within models (i.e < 0.2), and the high NO_x levels, little effect on average radical diurnals was seen by adding in HO_2 aerosol uptake into the model. Figure 6 shows that the OH and RO_2 radical concentrations were not significantly affected on average across the campaign by the addition of aerosol uptake. The average median diurnal of HO_2 can be seen as slightly

decreased, i.e. the over-prediction of HO_2 is slightly less for MCM_gamma compared to MCM_base, with the over-prediction decreasing from a factor of ~2.9 to ~2.4 at the 14:30 peak in the diurnal.

Due to the recycling of RO_2 to HO_2 and then back to OH by NO, it is important to consider the dependency of radicals on NO and whether the addition of the HO_2 uptake coefficient has an effect on the model's ability to predict the dependency of radical concentrations on NO. The dependency of measured/modelled OH, HO_2 and RO_2 on NO mixing ratio is discussed fully for the MCM_base model in Whalley et al., 2021, and is compared to MCM_gamma in Figure 2 of Supplementary Information.

To showcase any effect adding HO_2 aerosol uptake would have on HO_2 loss pathways as a whole, and thereby make a judgement on the effect of decreased $PM_{2.5}$ and hence HO_2 loss via aerosol surfaces on the O_3 production within Beijing, a rate of destruction analysis (RODA) was done for MCM_gamma. The loss pathways of HO_2 within MCM_gamma are shown in Figure 7 as an average median diurnal and as a function of NO mixing ratio (ppb), in addition to the percentage contribution of HO_2 uptake to the overall loss of HO_2 within the model.

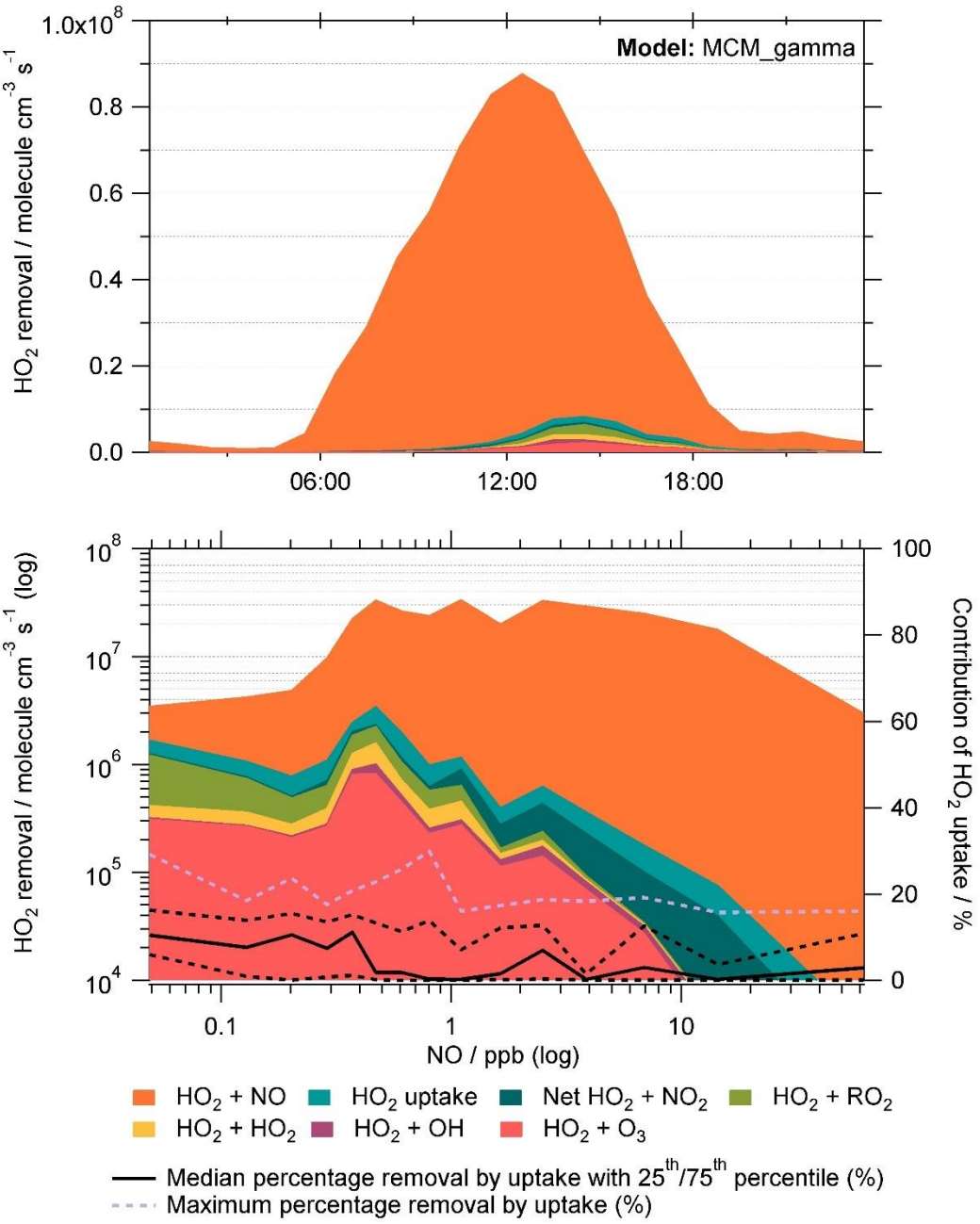

Figure 7. Rate of destruction analysis (RODA) showing the dominant loss pathways of HO_2 within MCM_gamma shown as (a) a diurnal variation and (b) as a function of NO mixing ratio (ppb). Median removal of HO_2 by uptake (%) as a function of NO (ppb) is shown as solid black line in (b), with $25^{th}/75^{th}$ percentile shown as the black dashed lines. Maximum percentage removal by uptake for a given NO mixing ratio is shown as a lilac dashed line.

As shown in the RODA, the dominant loss pathway of HO_2 is HO_2 + NO across the entire campaign (90 ± 14 % of total loss), followed by HO_2 + RO_2 (3.5 ± 8.1 % of total loss). This is expected due to high levels of NO_x in Beijing, especially during the day. As seen in the RODA diurnal, the HO_2 + NO loss pathway peaks at midday following the morning peak in NO mixing ratio due to rush hour traffic. As NO mixing ratio decreases, the relative importance of other

loss pathways of HO_2 increases. At the lowest NO mixing ratio, i.e. < 0.1 ppb NO, the loss pathways of HO_2 within MCM_gamma with the largest contribution to total loss were HO_2 + NO (55 ± 19 %), HO_2 + RO_2 (23 ± 17 %) and HO_2 + O_3 (9.3 ± 4.1 %). It is worth noting that as the NO mixing ratio decreases the relative importance of HO_2 removal by O_3 increases presumably due to the titration reaction of O_3 with NO decreasing (and hence higher observed [O_3]). This could be important when considering policy changes with NO_x pollution in China decreasing in recent years. The contribution of the various loss pathways of HO_2 to total HO_2 loss within MCM_gamma under low (< 0.1 ppb) and high (>0.1 ppb) NO are compared in Table 4.

	HO_2+O_3	**HO_2+OH**	**HO_2+HO_2**	**HO_2+RO_2**	**Net HO_2+NO_2**	**HO_2+NO**	**uptake**
Low NO (< 0.1 ppb)	9.3 ± 4.1	0.1 ± 0.1	3.0 ± 1.8	23 ± 17	2.4 ± 3.0	55 ± 19	7.3 ± 7.3
High NO (> 0.1 ppb)	1.8 ± 2.3	0.2 ± 0.3	0.8 ± 1.3	2.0 ± 4.4	0.4 ± 1.2	93 ± 9.0	1.9 ± <0.01

Table 4. Average relative percentage contribution of individual HO_2 loss pathways to the total loss of HO_2 within MCM_gamma, averaged for days when NO was low, (< 0.1 ppb) and high (> 0.1 ppb). Net HO_2+NO_2 refers to HO_2+NO_2→HO_2NO_2 minus HO_2NO_2→HO_2+NO_2.

Though there is not a strong dependence of HO_2 aerosol uptake loss pathway on NO mixing ratio for the calculated γ_{HO_2} (av. 0.07 ± 0.035) within MCM_gamma, it can be seen that at the lowest NO mixing ratios an average of ~7 % of total HO_2 loss is due to uptake, with a maximum at the lowest NO of ~29% (shown as lilac dashed line in Figure 7). This is a significant loss of HO_2, especially on days where the NO mixing ratio is low and the aerosol surface area is high, highlighting that the uptake of HO_2 onto aerosols could be important, and will be increasingly so at lower NO.

3.3.2 Comparison to γ_{HO_2} fixed at 0.2

While the maximum γ_{HO_2} calculated using the Song parameterisation for the summer AIRPRO campaign was 0.15, to provide context with previous modelling studies, the commonly used fixed value of γ_{HO_2}= 0.2 was added into the MCM_base model to give the MCM_SA model. The average median diurnals of modelled OH, HO_2 and RO_2 (molecule cm^{-3}) for MCM_base, MCM_gamma and MCM_SA are shown in Figure 6.

In comparison to calculated γ_{HO_2} in MCM_gamma, a fixed γ_{HO_2}= 0.2 had a more significant effect on radical concentrations. While the median diurnal shows that the RO_2 concentration was not significantly affected by the addition of HO_2 uptake, the over-prediction seen in the average median HO_2 concentration compared to the measurements at the 14:30 peak decreased

from a factor of ~2.9 in MCM_base to ~2.3. A plot of measured to modelling ratio of HO_2 as a function of aerosol surface area is shown in Figure 4 of Supplementary Information for both MCM_gamma and MCM_SA. OH radical concentrations were still relatively well reproduced with early afternoon OH concentrations predicted better though this is due to a shift in the modelled peak compared to the measured concentration peaking at midday. The ability of the model to reproduce the NO dependence of radical concentrations with the addition of γ_{HO_2}= 0.2 is discussed in Section 1.3 of Supplementary Information.

Analysis of the RODA for MCM_SA shows that with γ_{HO_2}= 0.2 HO_2 aerosol uptake is a significant contributor to total loss of HO_2 (8.1 ± 13 %, averaged for all NO mixing ratios). However, for all NO mixing ratios HO_2 + NO is still the dominant loss pathway (86 ± 18 %), as expected. At the lowest NO mixing ratios (i.e. < 0.1 ppb) an average of ~29 % of total HO_2 loss is due to uptake, with a maximum at the lowest NO of ~78%, shown in Figure 8. The contribution of the various loss pathways of HO_2 to total HO_2 loss within MCM_gamma under low (< 0.1 ppb) and high (>0.1 ppb) NO are compared in Table 5. The comparison of percentage contribution of HO_2 uptake to total HO_2 removal binned against NO mixing ratio (ppb) for MCM_gamma and MCM_SA RODA is shown in Figure 8.

	HO_2+O_3	**HO_2+OH**	**HO_2+HO_2**	**HO_2+RO_2**	**Net HO_2+NO_2**	**HO_2+NO**	**uptake**
Low NO (< 0.1 ppb)	6.9 ± 3.5	0.1 ± 0.1	1.7 ± 1.4	17 ± 14	1.6 ± 2.2	44 ± 24	29 ± 24
High NO (> 0.1 ppb)	1.8 ± 2.1	0.2 ± 0.2	0.6 ± 1.0	1.7 ± 3.8	0.4 ± 1.0	89 ± 13	6.5 ± 9.7

Table 5. Average relative percentage contribution of individual HO_2 loss pathways to the total loss of HO_2 within MCM_SA (fixed γ_{HO_2} = 0.2), averaged for days when NO was low, (< 0.1 ppb) and high (> 0.1 ppb). Net HO_2+NO_2 refers to HO_2+NO_2→HO_2NO_2 minus HO_2NO_2→HO_2+NO_2.

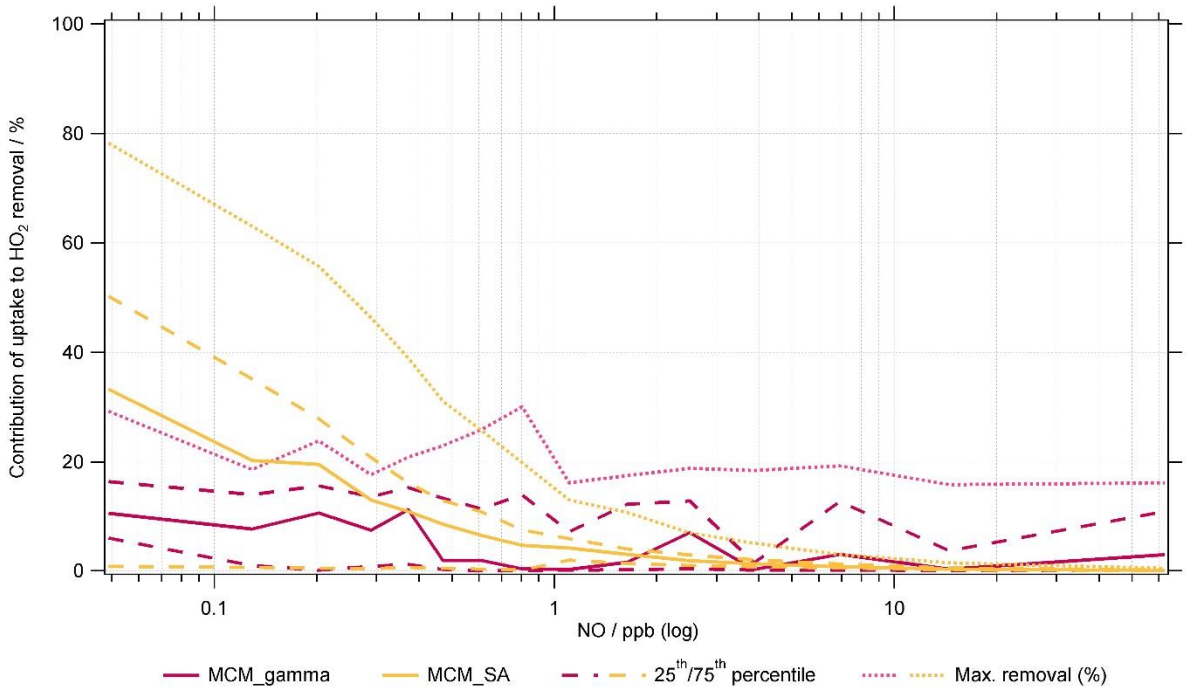

Figure 8. Average percentage contribution of HO_2 uptake to total HO_2 removal within MCM_gamma (pink line, γ_{HO_2}= 0.070 ± 0.035) and MCM_SA model (yellow line, γ_{HO_2} = 0.2) for Summer AIRPRO campaign plotted as a function of NO mixing ratio (ppb). Dashed lines represent the 25th/75th percentiles. Dotted lines represent maximum removal.

3.3.3 Effect of γ_{HO_2} on the O_3 regime

$\frac{L_N}{Q}$ was calculated for all model runs, MCM_base, MCM_gamma and MCM_SA using modelled [HO_2] and [RO_2] concentrations but measured values of [NO] and [NO_2], to investigate the effect on the O_3 regime of adding HO_2 aerosol uptake into the model. The time series of calculated $\frac{L_N}{Q}$ for all models, in addition to the regime transition point, $\frac{L_N}{Q_{trans}}$ for the entire campaign is shown in Figure 9.

When $\frac{L_N}{Q}<\frac{L_N}{Q_{trans}}$, this is defined as a NO_x-sensitive regime, meaning that small changes in NO_x will affect the rate of in situ O_3 production. This can be seen on a few days across the campaign, specifically in the afternoon, due to NO_x peaking in the morning due to traffic emissions before rapidly decreasing in the afternoon which pushes the O_3 regime on certain days from VOC-limited to NO_x-limited. However, for the majority of the campaign, the O_3 production regime is VOC-limited, for all models, meaning that O_3 production rates will not be significantly affected by small changes in NO_x.

Binning $\frac{L_N}{Q}$ against NO mixing ratio (ppb), in Figure 10, shows the change from VOC to NO_x-limited regime at very low NO mixing ratios for MCM_base, MCM_gamma and MCM_SA. As aerosol uptake is added the transition to NO_x-limited regime occurs at higher NO, with average median transition point occurring at ~ 0.2 ppb NO for MCM_gamma (average γ_{HO_2}= 0.070 ± 0.035) and at ~0.5 ppb NO for MCM_SA (fixed γ_{HO_2}= 0.2). This suggests that a reduction in PM (and therefore uptake of HO_2 onto aerosols) would delay the transition to a NO_x-sensitive regime until lower NO_x levels are reached. Therefore, any emissions policy aimed at reduced NO_x to decrease O_3 levels would not be as effective if PM is decreasing at the same time.

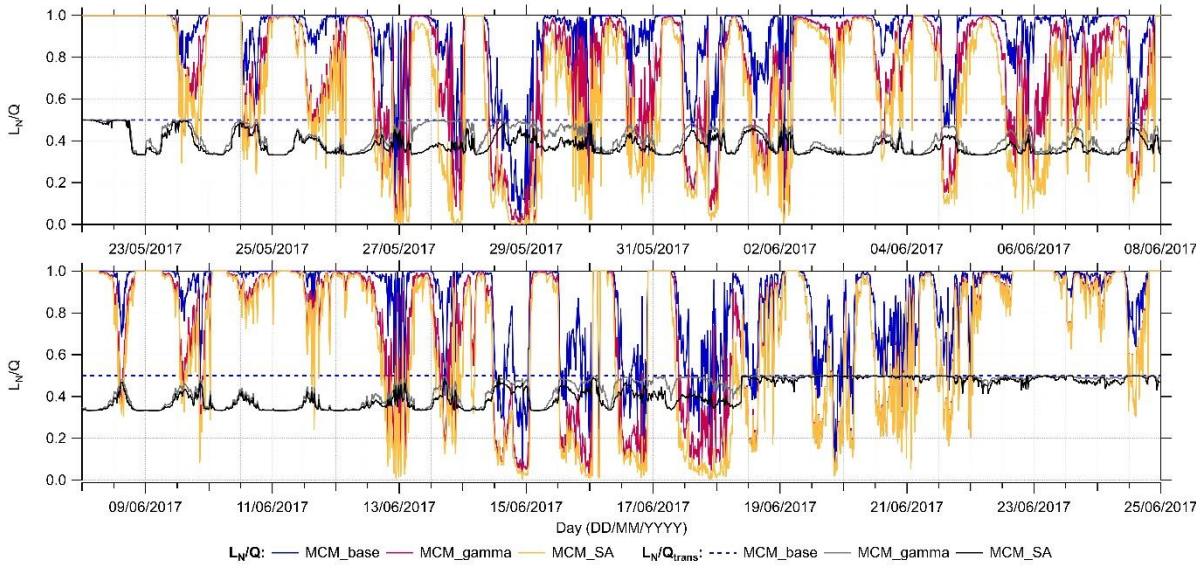

Figure 9. Time series of calculated $\frac{L_N}{Q}$ and $\frac{L_N}{Q_{trans}}$values for MCM_base (blue), MCM_gamma (pink) and MCM_SA (yellow) models across the entire summer AIRPRO campaign. $\frac{L_N}{Q_{trans}}$ for MCM_gamma is shown as grey line, while $\frac{L_N}{Q_{trans}}$ for MCM_SA is the black line.

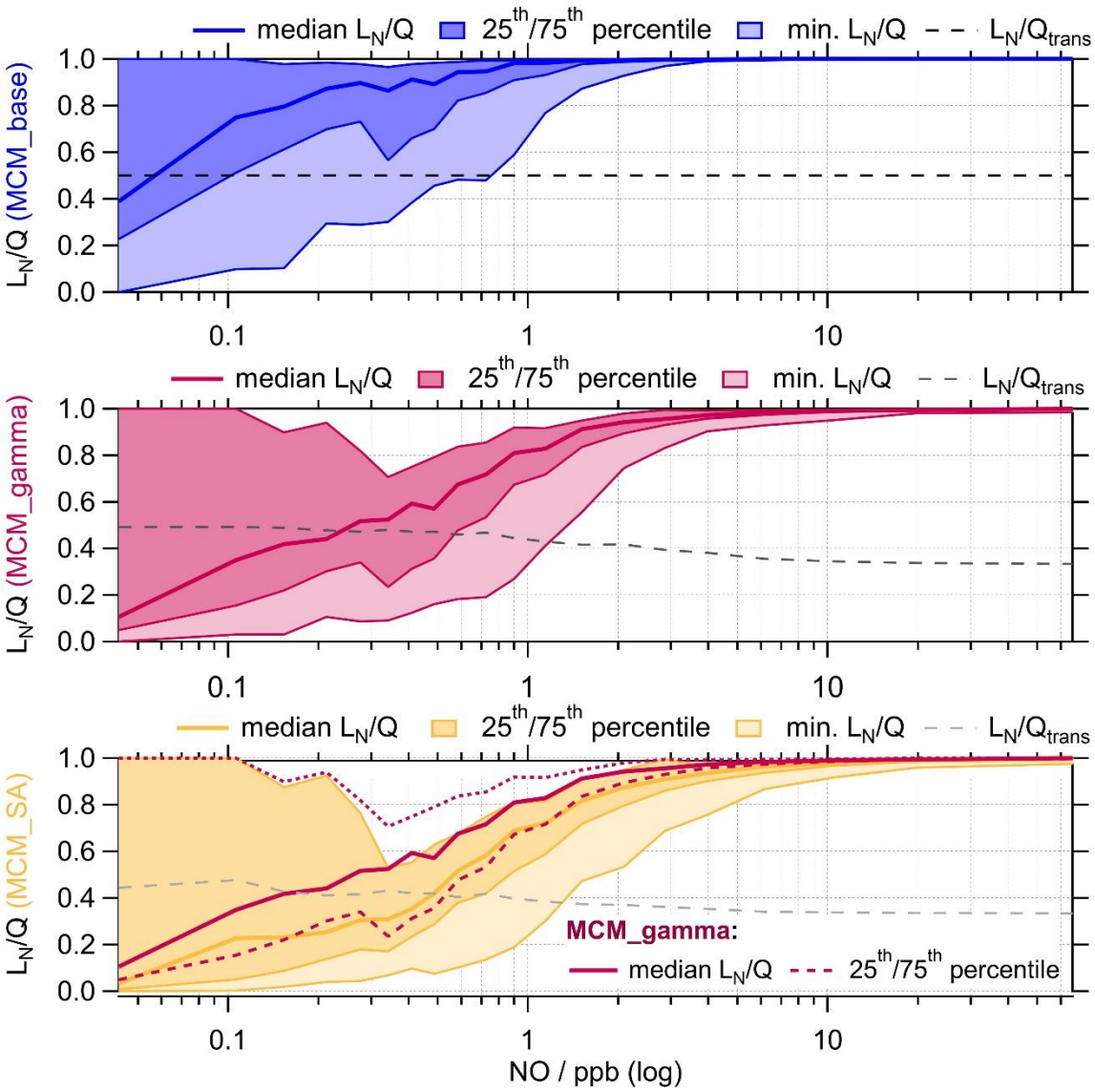

Figure 10. $\frac{L_N}{Q}$ for MCM_base (blue, top panel), MCM_gamma (pink, middle panel) and MCM_SA (yellow, bottom panel) binned against the log of measured NO mixing ratio for the entire summer AIRPRO campaign. $\frac{L_N}{Q_{trans}}$ for MCM_base (black dashed line) taken as 0.5 for entire range of NO mixing ratios. $\frac{L_N}{Q_{trans}}$ for MCM_gamma (dark grey dashed line) and MCM_SA (light grey dashed line) calculated using equation 10. $25^{th}/75^{th}$ percentiles and minimum $\frac{L_N}{Q}$ are plotted to show full spread of data for each model scenario.

The average median diurnal of absolute $P(O_3)$, $\frac{\delta P(O_3)}{\delta \ln [X]}$, for the MCM_gamma and MCM_SA over the entire campaign is shown in Figure 11. The time series of absolute $P(O_3)$, averaged up to a daily time resolution, across the entire measurement period can be found in Supplementary Information as SI Figure 5.

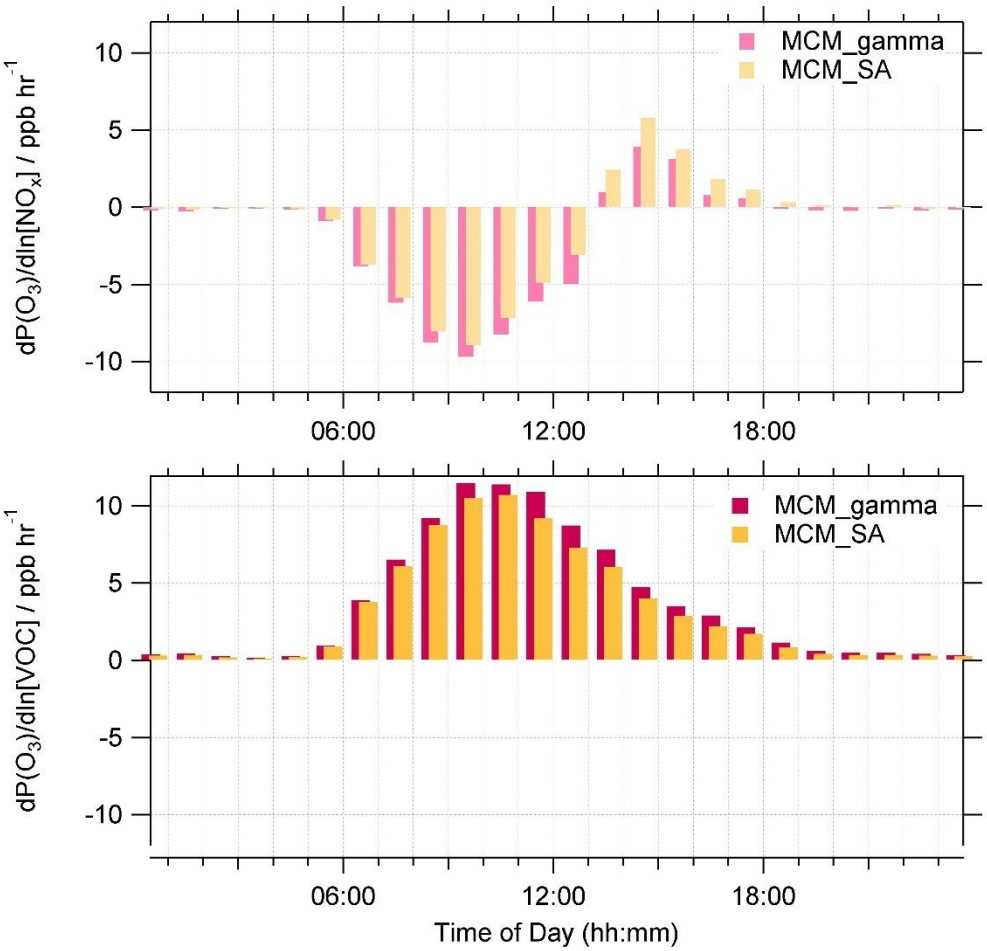

Figure 11. Average median diurnal of absolute O_3 sensitivity to NO_x (top panel) and VOC (bottom panel) in ppbV h^{-1} for MCM_gamma (pink) and MCM_SA (yellow) across the entire summer AIRPRO campaign. MCM_gamma includes γ_{HO_2} calculated using the Song parameterisation (av. 0.070 ± 0.035) while MCM_SA includes γ_{HO_2} at a fixed value of 0.2. All diurnals are 60 minute averages.

As expected from $\frac{L_N}{Q}$ calculations, calculations of absolute O_3 production sensitivity showcase that for both MCM_gamma and MCM_SA, on average, the O_3 regime was VOC sensitive throughout the day with NO_x sensitivity increasing in the afternoons. On a few days, when low NO mixing ratio coincided with high SA, the O_3 regime can be seen shifting from VOC to NO_x limited. An example of this can be found in SI Figure 6, for the 17/06/2017 and 18/06/2017 when the average NO mixing ratio was 0.41 ± 0.50 ppb and the average SA was (8.4 ± 6.2) × 10^{-6} cm^2 cm^{-3}. With an increase in γ_{HO_2} between MCM_gamma and MCM_SA, the sensitivity of O_3 regime to VOC decreased but sensitivity to NO_x increased. This effect could be important for areas where O_3 production regime is NO_x sensitive or less strongly VOC sensitive. With NO_x levels reportedly decreasing across China in recent years (Krotkov et al., 2016; Liu et al., 2016; Miyazaki et al., 2017; Van Der A et al., 2017), O_3 production regimes would be expected to move more towards NO_x-sensitive regimes in urban China. However, with concomitant

reduction in PM (Ma et al., 2016b; Lin et al., 2018), this transition to a NO_x-sensitive regime may be delayed until lower NO_x levels are reached.

Our result for the Beijing campaign are consistent with the results of Song et al., 2022 which concluded that for the conditions of the Wangdu campaign the addition of HO_2 uptake does not change the overall O_3 sensitivity regime throughout the campaign. However, the shift in O_3 sensitivity regime from VOC-limited to NO_x-limited from the consideration of HO_2 uptake could be important for areas with lower NO_x and high aerosol particle loading.

4 Conclusions

Using the Song parameterisation, the heterogeneous uptake coefficient of HO_2, γ_{HO_2}, was calculated for the summer AIRPRO campaign in Beijing, 2017 as a function of measured $[Cu^{2+}]_{eff}$, [ALWC] and [PM]. The calculated average $\gamma_{HO_2} = 0.070 \pm 0.035$ (ranging from 0.002 to 0.15 across the campaign) was significantly lower than the fixed value of $\gamma_{HO_2} = 0.2$ commonly used in modelling studies. This calculated value was similar, however, to values calculated for the Wangdu 2014 summer campaign in China (Tan et al., 2020; Song et al., 2020). Using the calculated γ_{HO_2}, the OH, HO_2 and RO_2 radical concentrations were modelled using the Master Chemical Mechanism, and compared to the measured campaign values, with and without the addition of HO_2 aerosol uptake. Due to the low calculated value of γ_{HO_2}, and the high levels of NO, rate of destruction analysis showed the dominant HO_2 loss pathway to be HO_2 + NO for all NO mixing ratios with HO_2 uptake not contributing significantly to the loss of HO_2 (< 2 %). However, at the lowest NO mixing ratios (i.e. < 0.1 ppb) HO_2 loss onto aerosols contributed up to a maximum of 29 % of the total HO_2 loss. Using the modelled HO_2 and RO_2 radical concentrations for model scenarios with and without HO_2 uptake, showed that on average the O_3 production regime was VOC-limited across the entire campaign with the exception of several days with low NO mixing ratio where the regime tended towards NO_x-limited, meaning that small changes in NO_x would not have a large effect on the O_3 production for this summer period in Beijing, however changes in HO_2 uptake could. While the addition of the calculated uptake coefficient did not change the overall O_3 regime across the campaign, with the O_3 production regime remaining strongly VOC-limited, the transition from a VOC-sensitive to NO_x-sensitive O_3 regime occurs at higher NO_x. This means that for Beijing, where the O_3 production regime is strongly VOC-sensitive and NO_x levels are high, any policy looking to reduce O_3 via the reduction of NO_x needs to consider concurrent PM reduction policies which may affect HO_2 uptake. In cleaner environments, where NO_x levels are lower,

but aerosol surface area is still high, lower values of γ_{HO_2}, i.e. less than 0.2, could have a more significant effect on both overall HO_2 concentration and the O_3 production regime.

Data availability. Data presented in this study can be obtained from authors upon request (d.e.heard@leeds.ac.uk)

Author contributions. LKW, EJS, RWM, CY and DEH carried out the radical measurements. LKW and EJS developed the model and JED performed the calculations. JDL, FS, JRH, RED, MS, JFH, ACL, AM, SDW, AB, TJB, HC, BO, CJP, CNH, RLJ, LRC, LJK, WJFA, WJB, SS, JX, TV, ZS, RMH, SK, SG, YS, WX, SY, LW, PF and XW provided logistical support and supporting data to constrain the model. JED prepared the manuscript with contributions from all co-authors.

Competing interests. The authors declare that they have no conflict of interest.

Acknowledgements. We are grateful to the Natural Environmental Research Council for funding a SPHERES PhD studentship (Joanna E. Dyson). We are grateful to Tuan Vu for providing supervision and supporting data.

5 References

Bohn, B., Heard, D. E., Mihalopoulos, N., Plass-Dülmer, C., Schmitt, R., and Whalley, L. K.: Characterisation and improvement of j(O^1D) filter radiometers, Atmos. Meas. Tech., 9, 3455-3466, https://doi.org/10.5194/amt-9-3455-2016, 2016.

Brauer, M., Freedman, G., Frostad, J., van Donkelaar, A., Martin, R. V., Dentener, F., Dingenen, R. v., Estep, K., Amini, H., Apte, J. S., Balakrishnan, K., Barregard, L., Broday, D., Feigin, V., Ghosh, S., Hopke, P. K., Knibbs, L. D., Kokubo, Y., Liu, Y., Ma, S., Morawska, L., Sangrador, J. L. T., Shaddick, G., Anderson, H. R., Vos, T., Forouzanfar, M. H., Burnett, R. T., and Cohen, A.: Ambient Air Pollution Exposure Estimation for the Global Burden of Disease 2013, Environ. Sci. Technol., 50, 79-88, https://doi.org/10.1021/acs.est.5b03709, 2016.

Commane, R., Floquet, C. F. A., Ingham, T., Stone, D., Evan, M. J., and Heard, D. E.: Observations of OH and HO_2 radicals over West Africa, Atmos. Chem. Phys., 10, 8783-8801, https://doi.org/10.5194/acp-10-8783-2010, 2010.

Cooper, P. L. and Abbatt, J. P. D.: Heterogeneous Interactions of OH and HO2 Radicals with Surfaces Characteristic of Atmospheric Particulate Matter, The Journal of Physical Chemistry, 100, 2249-2254, https://doi.org/10.1021/jp952142z, 1996.

660 Crilley, L. R., Kramer, L., Pope, F. D., Whalley, L. K., Cryer, D. R., Heard, D. E., Lee, J. D.,
661 Reed, C., and Bloss, W. J.: On the interpretation of in situ HONO observations via
662 photochemical steady state, Faraday Discuss., 189, 191-212,
663 https://doi.org/10.1039/c5fd00224a, 2016.
664 Dunmore, R., Hopkins, J., Lidster, R., Lee, J., Evans, M., Rickard, A., Lewis, A., and
665 Hamilton, J.: Diesel-related hydrocarbons can dominate gas phase reactive carbon in
666 megacities, Atmos. Chem. Phys., 15, 9983-9996, https://doi.org/10.5194/acp-15-9983-2015,
667 2015.
668 Forster, P., Ramaswamy, V., Artaxo, P., Berntsen, T., Betts, R., Fahey, D. W., Haywood, J.,
669 Lean, J., Lowe, D. C., Myhre, G., Nganga, J., Prinn, R., Raga, G., Schulz, M., and Dorland,
670 R. V.: Chapter 2. Changes in atmospheric constituents and in radiative forcing. , Climate
671 Change 2007. The Physical Science Basis, 2007.
672 Fountoukis, C. and Nenes, A.: ISORROPIA II: a computationally efficient thermodynamic
673 equilibrium model for K^+-Ca^{2+}-Mg^{2+}-NH_4^+-Na^+-SO_4^{2-}-NO_3^--Cl^--H_2O aerosols, Atmos. Chem.
674 Phys., 7, 4639-4659, https://doi.org/10.5194/acp-7-4639-2007, 2007.
675 Gakidou, E., Afshin, A., Abajobir, A. A., Abate, K. H., Abbafati, C., Abbas, K. M., Abd-
676 Allah, F., Abdulle, A. M., Abera, S. F., and Aboyans, V.: Global, regional, and national
677 comparative risk assessment of 84 behavioural, environmental and occupational, and
678 metabolic risks or clusters of risks, 1990–2016: a systematic analysis for the Global Burden
679 of Disease Study 2016, The Lancet, 390, 1345-1422, https://doi.org/10.1016/S0140-
680 6736(18)32279-7, 2017.
681 George, I. J., Matthews, P. S. J., Whalley, L. K., Brooks, B., Goddard, A., Baeza-Romero,
682 M., and Heard, D. E.: Measurements of uptake coefficients for heterogeneous loss of HO_2
683 onto submicron inorganic salt aerosols., Phys. Chem. Chem. Phys., 15, 12829-12845,
684 https://doi.org/10.1039/c3cp51831k, 2013.
685 Hopkins, J. R., Jones, C. E., and Lewis, A. C.: A dual channel gas chromatograph for
686 atmospheric analysis of volatile organic compounds including oxygenated and monoterpene
687 compounds., J. Environ. Monit., 13, 2268-2276, https://doi.org/10.1039/C1EM10050E, 2011.
688 Ivatt, P. D., Evans, M. J., and Lewis, A. C.: Suppression of surface ozone by an aerosol-
689 inhibited photochemical ozone regime, Nat. Geosci, 15, 536-540,
690 https://doi.org/10.1038/s41561-022-00972-9, 2022.
691 Jacob, D. J.: Heterogeneous chemistry and tropospheric ozone, Atmos. Environ., 34, 2131-
692 2159, https://doi.org/10.1016/S1352-2310(99)00462-8, 2000.

693 Jin, Y., Andersson, H., and Zhang, S.: Air Pollution Control Policies in China: A
694 Retrospective and Prospects, Int. J. Environ. Res. Public Health, 13,
695 https://doi.org/10.3390/ijerph13121219, 2016.
696 Kanaya, Y. G., Cao, R. Q., Kato, S. G., Miyakawa, Y. K., Kajii, Y., Tanimoto, H., Yokouchi,
697 Y., Mochida, M., Kawamura, K., and Akimoto, H.: Chemistry of OH and HO_2 radicals
698 observed at Rishiri Island, Japan, in September 2003: Missing daytime sink of HO_2 and
699 positive nighttime correlations with monoterpenes, J. Geophys. Res. Atmos., 112, D11308,
700 https://doi.org/10.1029/2006JD007987, 2007.
701 Kleinman, L. I.: Ozone process insights from field experiments – part II: Observation-based
702 analysis for ozone production, Atmos. Environ., 34, 2023-2033,
703 https://doi.org/10.1016/S1352-2310(99)00457-4, 2000.
704 Kleinman, L. I., Daum, P. H., Lee, Y.-N., Nunnermacker, L. J., Springston, S. R., Weinstein-
705 Lloyd, J., and Rudolph, J.: Sensitivity of ozone production rate to ozone precursors, Geophys.
706 Res. Lett., 28, 2903-2906, https://doi.org/10.1029/2000GL012597, 2001.
707 Kleinman, L. I., Daum, P. H., Lee, J. H., Lee, Y.-N., Nunnermacker, L. J., Springston, S. R.,
708 Newman, L., Weinstein-Lloyd, J., and Sillman, S.: Dependence of ozone production on NO
709 and hydrocarbons in the troposphere, Geophys. Res. Lett., 24, 2299-2302,
710 https://doi.org/10.1029/97GL02279, 1997.
711 Krotkov, N. A., McLinden, C. A., Li, C., Lamsal, L. N., Celarier, E. A., Marchenko, S. V.,
712 Swartz, W. H., Bucsela, E. J., Joiner, J., Duncan, B. N., Boersma, K. F., Veefkind, J. P.,
713 Levelt, P. F., Fioletov, V. E., Dickerson, R. R., He, H., Lu, Z., and Streets, D. G.: Aura OMI
714 observations of regional SO_2 and NO_2 pollution changes from 2005 to 2015, Atmos. Chem.
715 Phys., 16, 4605-4629, https://doi.org/10.5194/acp-16-4605-2016, 2016.
716 Lakey, P. S. J., George, I. J., Baeza-Romero, M., Whalley, L. K., and Heard, D. E.: Organics
717 substantially reduce HO_2 uptake onto aerosols containing transition metal ions. , J. Phys.
718 Chem. A, 120, 1421-1430, https://doi.org/10.1021/acs.jcpa.5b06316, 2016.
719 Lakey, P. S. J., George, I. J., Whalley, L. K., Baeza-Romero, M., and Heard, D. E.:
720 Measurements of HO_2 uptake coefficients onto single component organic aerosols.,
721 Environmental Science Technology, 49, 4878-4885, https://doi.org/10.1021/acs.est.5b00948,
722 2015.
723 Le Breton, M., Bacak, A., Muller, J. B. A., Bannan, T. J., Kennedy, O., Ouyang, B., Xiao, P.,
724 Bauguitte, S. J. B., Shallcross, D. E., Jones, R. L., Daniels, M. J. S., Ball, S. M., and Percival,
725 C. J.: The first airborne comparison of N_2O_5 measurements over the UK using a CIMS and

BBCEAS during the RONOCO campaign, Analytical Methods, 6, 9731-9743, https://doi.org/10.1039/C4AY02273D, 2014.
Levy, H.: Normal atmosphere: large radical and formaldehyde concentrations predicted, Science, 173, 141-143, https://doi.org/10.1126/science.173.3992.141, 1971.
Li, H., Wang, D., Cui, L., Gao, Y., Huo, J., Wang, X., Zhang, Z., Tan, Y., Huang, Y., and Cao, J. J. S. o. t. t. e.: Characteristics of atmospheric PM2. 5 composition during the implementation of stringent pollution control measures in shanghai for the 2016 G20 summit, 648, 1121-1129, https://doi.org/10.1016/j.scitotenv.2018.08.219, 2019.
Li, K., Jacob, D. J., Liao, H., Shen, L., Zhang, Q., and Bates, K.: Anthropogenic drivers of 2013-2017 trends in summer surface ozone in China, Proceedings of the National Academy of Sciences, 116, 422-427, https://doi/org/10.1073/pnas.1812168116, 2018.
Lin, C. Q., Liu, G., Lau, A. K. H., Li, Y., Li, C. C., Fung, J. C. H., and Lao, X. Q.: High-resolution satellite remote sensing of provincial $PM_{2.5}$ trends in China from 2001 to 2015, Atmos. Environ., 180, 110-116, https://doi.org/10.1016/j.atmosenv.2018.02.045, 2018.
Liu, F., Zhang, Q., van der A, R. J., Zheng, B., Tong, D., Yan, L., Zheng, Y., and He, K.: Recent reduction in NO_x emissions over China: synthesis of satellite observations and emission inventories, Environ. Res. Lett, 11, 114002, https://doi.org/10.1088/1748-9326/11/11/114002, 2016.
Liu, Y.-H., Liao, W.-Y., Lin, X.-F., Li, L., and Zeng, X.-l.: Assessment of Co-benefits of vehicle emission reduction measures for 2015–2020 in the Pearl River Delta region, China, Environ. Pollut., 223, 62-72, https://doi.org/10.1016/j.envpol.2016.12.031, 2017.
Ma, Z., Xu, J., Quan, W., Zhang, Z., Lin, W., and Xu, X.: Significant increase of surface ozone at a rural site, north of eastern China, Atmos. Chem. Phys., 16, 3969-3977, https://doi.org/10.5194/acp-16-3969-2016, 2016a.
Ma, Z., Hu, X., Sayer, A. M., Levy, R., Zhang, Q., Xue, Y., Tong, S., Bi, J., Huang, L., and Liu, Y.: Satellite-Based Spatiotemporal Trends in $PM_{2.5}$ Concentrations: China, 2004-2013, Environ. Health Perspect., 124, 184-192, https://doi.org/10.1289/ehp.1409481, 2016b.
Mao, J., Fan, S., Jacob, D. J., and Travis, K. R.: Radical loss in the atmosphere from Cu-Fe redox coupling in aerosols, Atmos. Chem. Phys., 13, 509-519, https://doi.org/10.5194/acp-13-509-2013, 2013.
Mao, J., Jacob, D. J., Evans, M. J., Olson, J. R., Ren, X., Brune, W. H., Chair, J. M. S., Crounse, J. D., Spencer, K. M., Beaver, M. R., Wennberg, P. O., Cubison, M. J., Jimenez, J. L., Fried, A., Weibring, P., Walega, J. G., Hall, S. R., Weinheimer, A. J., Cohen, R. C., Chen, G., Crawford, J. H., McHaughton, C., Clarke, A. D., Jaegle, L., Fisher, J. K., Yantosca, R.

M., LeSager, P., and Carouge, C.: Chemsitry of hydrogen oxide radicals (HO_x) in the artic troposphere in spring, Atmos. Chem. Phys., 10, 5823-5838, https://doi.org/10.5194/acp-10-5823-2010, 2010.

Martinez, M., Harder, H., Kovacs, T. A., Simpas, J. B., Bassis, J., Lesher, R., Brune, W. H., Frost, G. J., Williams, E. J., Stroud, C. A., Jobson, B. T., Roberts, J. M., Hall, S. R., Shetter, R. E., Wert, B., Fried, A., Alicke, B., Stutz, J., Young, V. L., White, A. B., and Zamora, R. J.: OH and HO_2 concentrations, sources, and loss rates during the Southern Oxidants Study in Nashville, Tennessee, summer 1999, Journal of Geophysical Research: Atmospheres, 108, https://doi.org/10.1029/2003JD003551, 2003.

Matthews, P. S. J., Baeza-Romero, M., Whalley, L. K., and Heard, D. E.: Uptake of HO_2 radicals onto Arizona test dust particles using an aerosol flow tube, Atmos. Chem. Phys., 14, 7397-7408, https://doi.org/10.5194/acp-14-7397-2014, 2014.

Miyazaki, K., Eskes, H., Sudo, K., Boersma, K. F., Bowman, K., and Kanaya, Y.: Decadal changes in global surface NO_x emissions from multi-constituent satellite data assimilation, Atmos. Chem. Phys., 17, 807-837, https://doi.org/10.5194/acp-17-807-2017, 2017.

Mozurkewich, M., McMurry, P. H., Gupta, A., and Calvert, J. G.: Mass accommodation coefficient for HO_2 radicals on aqueous particles, J. Geophys. Res., 92, 4163-4170, https://doi.org/10.1029/JD092iD04p04163, 1987.

Sakamoto, Y., Sadanaga, Y., Li, J., Matsuoka, K., Takemura, M., Fujii, T., Nakagawa, M., Kohno, N., Nakashima, Y., Sato, K., Nakayama, T., Kato, S., Takami, A., Yoshino, A., Murano, K., and Kajii, Y.: Relative and Absolute Sensitivity Analysis on Ozone Production in Tsukuba, a City in Japan, Environ. Sci. Technol., 53, 13629-13635, https://doi.org/10.1021/acs.est.9b03542, 2019.

Shi, Z., Vu, T., Kotthaus, S., Harrison, R. M., Grimmond, S., Yue, S., Zhu, T., Lee, J., Han, Y., Demuzere, M., Dunmore, R. E., Ren, L., Liu, D., Wang, Y., Wild, O., Allan, J., Acton, W. J., Barlow, J., Barratt, B., Beddows, D., Bloss, W. J., Calzolai, G., Carruthers, D., Carslaw, D. C., Chan, Q., Chatzidiakou, L., Chen, Y., Crilley, L., Coe, H., Dai, T., Doherty, R., Duan, F., Fu, P., Ge, B., Ge, M., Guan, D., Hamilton, J. F., He, K., Heal, M., Heard, D., Hewitt, C. N., Hollaway, M., Hu, M., Ji, D., Jiang, X., Jones, R., Kalberer, M., Kelly, F. J., Kramer, L., Langford, B., Lin, C., Lewis, A. C., Li, J., Li, W., Liu, H., Liu, J., Loh, M., Lu, K., Lucarelli, F., Mann, G., McFiggans, G., Miller, M. R., Mills, G., Monk, P., Nemitz, E., O'Connor, F., Ouyang, B., Palmer, P. I., Percival, C., Popoola, O., Reeves, C., Rickard, A. R., Shao, L., Shi, G., Spracklen, D., Stevenson, D., Sun, Y., Sun, Z., Tao, S., Tong, S., Wang, Q., Wang, W., Wang, X., Wang, X., Wang, Z., Wei, L., Whalley, L., Wu, X., Wu, Z., Xie, P.,

Yang, F., Zhang, Q., Zhang, Y., Zhang, Y., and Zheng, M.: Introduction to the special issue "In-depth study of air pollution sources and processes within Beijing and its surrounding region (APHH-Beijing)", Atmos. Chem. Phys., 19, 7519-7546, https://doi.org/10.5194/acp-19-7519-2019, 2019.

Silver, B., Reddington, C. L., Arnold, S. R., and Spracklen, D. V.: Substantial changes in air pollution across China during 2015–2017, Environ. Res. Lett, 13, 114012, https://doi.org/10.1088/1748-9326/aae718, 2018.

Slater, E. J.: Understanding radical chemistry in Beijing through observations and modelling, School of Chemistry, University of Leeds, 2020.

Slater, E. J., Whalley, L. K., Woodward-Massey, R., Ye, C., Lee, J. D., Squires, F., Hopkins, J. R., Dunmore, R. E., Shaw, M., Hamilton, J. F., Lewis, A. C., Crilley, L. R., Kramer, L., Bloss, W., Vu, T., Sun, Y., Xu, W., Yue, S., Ren, L., Acton, W. J. F., Hewitt, C. N., Wang, X., Fu, P., and Heard, D. E.: Elevated levels of OH observed in haze events during wintertime in central Beijing, Atmos. Chem. Phys. Discuss., 2020, 1-43, https://doi.org/10.5194/acp-2020-362, 2020.

Smith, K. R., Edwards, P. M., Evans, M. J., Lee, J. D., Shaw, M. D., Squires, F., Wilde, S., and Lewis, A. C.: Clustering approaches to improve the performance of low cost air pollution sensors, Faraday Discuss., 200, 621-637, https://doi.org/10.1039/C7FD00020K, 2017.

Sommariva, R., Haggerstone, A. L., Carpenter, L. J., Carslaw, N., Creasey, D. J., Heard, D. E., Lee, J. D., Lewsi, A. C., Pilling, M. J., and Zador, J.: OH and HO_2 chemistry in clean marine air during SOAPEX-2, Atmos. Chem. Phys., 4, 839-856, https://doi.org/10.5194/acp-4-839-2004, 2004.

Song, H., Lu, K., Dong, H., Tan, Z., Chen, S., Zeng, L., and Zhang, Y.: Reduced Aerosol Uptake of Hydroperoxyl Radical May Increase the Sensitivity of Ozone Production to Volatile Organic Compounds, Environ. Sci. Tech. Letts., 9, 22-29, https://doi.org/10.1021/acs.estlett.1c00893, 2022.

Song, H., Chen, X., Lu, K., Zou, Q., Tan, Z., Fuchs, H., Wiedensohler, A., Moon, D. R., Heard, D. E., Baeza-Romero, M. T., Zheng, M., Wahner, A., Kiendler-Scharr, A., and Zhang, Y.: Influence of aerosol copper on HO_2 uptake: a novel parameterized equation, Atmos. Chem. Phys., 20, 15835-15850, https://doi.org/10.5194/acp-20-15835-2020, 2020.

Stone, D., Whalley, L. K., Ingham, T., Edwards, P. M., Cryer, D. R., Brumby, C. A., Seakins, P. W., and Heard, D. E.: Measurement of OH reactivity by laser flash photolysis coupled with laser-induced fluorescence spectroscopy, Atmos. Meas. Tech., 9, 2827-2844, https://doi.org/10.5194/amt-9-2827-2016, 2016.

Taketani, F., Kanaya, Y., and Akimoto, H.: Kinetics of heterogeneous reactions of HO_2 radical at ambient concentration levels with $(NH_4)_2SO_4$ and NaCl aerosol particles., J. Phys. Chem. A, 112, 2370-2377, https://doi.org/10.1021/jp0769936, 2008.

Taketani, F., Kanaya, Y., Pocharnart, P., Liu, Y., Li, J., Okuzawa, K., Kawamura, K., Wang, Z., and Akimoto, H.: Measurement of overall uptake coefficients for HO_2 radicals by aerosol particles sampled from ambient air at Mts. Tai and Mang (China). Atmos. Chem. Phys., 12, 11907-11916, https://doi.org/10.5194/acp-12-11907-2012, 2012.

Tan, Z., Hofzumahaus, A., Lu, K., Brown, S. S., Holland, F., Huey, L. G., Kiendler-Scharr, A., Li, X., Liu, X., Ma, N., Min, K.-E., Rohrer, F., Shao, M., Wahner, A., Wang, Y., Wiedensohler, A., Wu, Y., Wu, Z., Zeng, L., Zhang, Y., and Fuchs, H.: No Evidence for a Significant Impact of Heterogeneous Chemistry on Radical Concentrations in the North China Plain in Summer 2014, Environ. Sci. Technol., 54, 5973-5979, https://doi.org/10.1021/acs.est.0c00525, 2020.

Thornton, J. A. and Abbatt, J. P. D.: Measurements of HO_2 uptake of aqueous aerosol: Mass accommodation coefficients and net reactive loss., J. Geophys. Res., 110, https://doi.org/10.1029/2004JD005402, 2005.

Thornton, J. A., Jaegle´, L., and McNeill, V. F.: Assessing known pathways for HO_2 loss in aqueous atmospheric aerosols: Regional and global impacts on tropospheric oxidants. , J. Geophys. Res., 113, https://doi.org/10.1029/2007JD009236, 2008.

van der A, R. J., Mijling, B., Ding, J., Koukouli, M. E., Liu, F., Li, Q., Mao, H., and Theys, N.: Cleaning up the air: effectiveness of air quality policy for SO_2 and NO_x emissions in China, Atmos. Chem. Phys., 17, 1775-1789, https://doi.org/10.5194/acp-17-1775-2017, 2017.

Verstraeten, W. W., Neu, J. L., Williams, J. E., Bowman, K. W., Worden, J. R., and Boersma, K. F.: Rapid increases in tropospheric ozone production and export from China, Nat. Geosci, 8, 690-695, https://doi.org/10.1038/ngeo2493, 2015.

Wang, P.: China's air pollution policies: Progress and challenges, Current Opinion in Environmental Science & Health, 19, 100227, https://doi.org/10.1016/j.coesh.2020.100227, 2021.

Whalley, L. K., Blitz, M. A., Desservattez, M., Seakins, P. W., and Heard, D. E.: Reporting the sensitivity of laser-induced fluorescence instruments used for HO_2 detection to an interference from RO_2 radicals and introducing a novel approach that enables HO_2 and certain RO_2 types to be selectively measured, Atmos. Meas. Tech., 6, 3425-3440, https://doi.org/10.5194/amt-6-3425-2013, 2013.

Whalley, L. K., Stone, D., Dunmore, R., Hamilton, J., Hopkins, J. R., Lee, J. D., Lewis, A. C., Williams, P., Kleffmann, J., Laufs, S., Woodward-Massey, R., and Heard, D. E.: Understanding in situ ozone production in the summertime through radical observations and modelling studies during the Clean air for London project (ClearfLo), Atmos. Chem. Phys., 18, 2547-2571, https://doi.org/10.5194/acp-18-2547-2018, 2018.

Whalley, L. K., Furneaux, K. L., Goddard, A., Lee, J. D., Mahajan, A., Oetjen, H., Read, K. A., Kaaden, N., Carpenter, L. J., Lewis, A. C., Plane, J. M. C., Saltzman, E. S., Wiedensohler, A., and Heard, D. E.: The chemistry of OH and HO_2 radicals in the boundary layer over the tropical Atlantic Ocean, Atmos. Chem. Phys., 10, 1555-1576, https://doi.org/10.5194/acp-10-1555-2010, 2010.

Whalley, L. K., Slater, E. J., Woodward-Massey, R., Ye, C., Lee, J. D., Squires, F., Hopkins, J. R., Dunmore, R. E., Shaw, M., Hamilton, J. F., Lewis, A. C., Mehra, A., Worrall, S. D., Bacak, A., Bannan, T. J., Coe, H., Ouyang, B., Jones, R. L., Crilley, L. R., Kramer, L. J., Bloss, W. J., Vu, T., Kotthaus, S., Grimmond, S., Sun, Y., Xu, W., Yue, S., Ren, L., Acton, W. J. F., Hewitt, C. N., Wang, X., Fu, P., and Heard, D. E.: Evaluating the sensitivity of radical chemistry and ozone formation to ambient VOCs and NOx in Beijing, Atmos. Chem. Phys. Discuss., 21, 2125-2147, https://doi.org/10.5194/acp-2020-785, 2021.

Wiedensohler, A., Birmili, W., Nowak, A., Sonntag, A., Weinhold, K., Merkel, M., Wehner, B., Tuch, T., Pfeifer, S., Fiebig, M., Fjäraa, A. M., Asmi, E., Sellegri, K., Depuy, R., Venzac, H., Villani, P., Laj, P., Aalto, P., Ogren, J. A., Swietlicki, E., Williams, P., Roldin, P., Quincey, P., Hüglin, C., Fierz-Schmidhauser, R., Gysel, M., Weingartner, E., Riccobono, F., Santos, S., Grüning, C., Faloon, K., Beddows, D., Harrison, R., Monahan, C., Jennings, S. G., O'Dowd, C. D., Marinoni, A., Horn, H. G., Keck, L., Jiang, J., Scheckman, J., McMurry, P. H., Deng, Z., Zhao, C. S., Moerman, M., Henzing, B., de Leeuw, G., Löschau, G., and Bastian, S.: Mobility particle size spectrometers: harmonization of technical standards and data structure to facilitate high quality long-term observations of atmospheric particle number size distributions, Atmos. Meas. Tech., 5, 657-685, https:/doi.org/10.5194/amt-5-657-2012, 2012.

Xue, L. K., Wang, T., Gao, J., Ding, A. J., Zhou, X. H., Blake, D. R., Wang, X. F., Saunders, S. M., Fan, S. J., Zuo, H. C., Zhang, Q. Z., and Wang, W. X.: Ground-level ozone in four Chinese cities: precursors, regional transport and heterogeneous processes, Atmos. Chem. Phys., 14, 13175-13188, https://doi.org/10.5194/acp-14-13175-2014, 2014.

Ye, C., Heard, D. E., and Whalley, L. K.: Evaluation of novel routes for NO_x formation in remote regions. , Environ. Sci. Technol., 51, 7442-7449, https://doi.org/acs.est.6b06441, 2017.

Zhou, J., Murano, K., Kohno, N., Sakamoto, Y., and Kajii, Y.: Real-time quantification of the total HO_2 reactivity of ambient air and HO_2 uptake kinetics onto ambient aerosols in Kyoto (Japan), Atmos. Environ., 223, 117189, https://doi.org/10.1016/j.atmosenv.2019.117189, 2020.

Zhou, J., Sato, K., Bai, Y., Fukusaki, Y., Kousa, Y., Ramasamy, S., Takami, A., Yoshino, A., Nakayama, T., Sadanaga, Y., Nakashima, Y., Li, J., Murano, K., Kohno, N., Sakamoto, Y., and Kajii, Y.: Kinetics and impacting factors of HO_2 uptake onto submicron atmospheric aerosols during the 2019 Air QUAlity Study (AQUAS) in Yokohama, Japan, Atmos. Chem. Phys., 21, 12243-12260, https://doi.org/10.5194/acp-21-12243-2021, 2021.